

Scalar dark matter with Z_3 symmetry in the type-II seesaw mechanism

XinXin Qi and Hao Sun^{*}

*Institute of Theoretical Physics, School of Physics, Dalian University of Technology,
No. 2 Linggong Road, Dalian, Liaoning, 116024, People's Republic of China*



(Received 14 November 2022; accepted 2 May 2023; published 17 May 2023)

We study a simple complex scalar singlet dark matter (DM) model with Z_3 symmetry in the framework of the type-II seesaw mechanism. We use the model to explain the excess of electron-positron flux measured by the AMS-02, DAMPE, and Fermi-LAT Collaborations, which is encouraged by the decay of the triplets produced from dark matter annihilations in the Galactic halo. We focus on the nondegenerate case in which the mass of DM is larger than that of the triplets' and deliberately alleviates the leptophilic properties of the DM, so that the semiannihilation effects are enhanced. With the guarantee of Z_3 symmetry, by fitting the antiproton spectrum observed in the PAMELA and AMS experiments, we find that the DM cubic terms and the couplings between DM and the Higgs boson are strongly constrained, leading to the semiannihilation cross-section fraction less than 11% when DM mass is given at 2 TeV.

DOI: [10.1103/PhysRevD.107.095026](https://doi.org/10.1103/PhysRevD.107.095026)

I. INTRODUCTION

So far, there are at least two unsolved problems in particle physics: the nature of dark matter (DM) proved by astronomical evidence [1–6] and the origin of the neutrino mass revealed by the observation of neutrino oscillations [7]. For dark matter, one of the most attractive candidates is the so-called weakly interacting massive particles, and the freeze-out mechanism can generate the observed dark matter relic density. Other paradigms of DM include strongly interacting massive particles (SIMPs) and forbidden dark matter, where SIMPs are realized by (effective) five-point self-interactions [8–11], and the latter is the annihilation of the hidden sector set opened at high temperature [8,12,13]. On the other hand, in order to understand the origin of neutrino mass theoretically, several mechanisms have been proposed, such as the type-I seesaw mechanism [14–16], by introducing heavy right-handed neutrinos, the type-II seesaw mechanism [17–24], by adding the $SU(2)$ Higgs triplet, and so on [25–28].

In this paper, we consider the dark matter issue as well as the neutrino mass issue in a common framework. For the settlement of DM, we introduce a complex scalar singlet (S) with a discrete Z_3 symmetry, and its Z_3 charge is unity ($X_S = 1$). While the standard model (SM) particles' are

zero ($X_{SM} = 0$), the stability of DM can therefore be guaranteed by the Z_3 symmetry. Such a type of extended singlet scalar could be naturally embedded in the $SO(10)$ group on account of the same gauge and $B - L$ quantum number compared with SM fermions. On the other hand, discrete symmetry such as Z_2 , Z_4 , or Z_N dark matter models have been presented in, for example, Refs. [29–35], where the common feature of such models is that the discrete symmetry could be the remnant symmetry of some breaking $U(1)_X$ gauge group [36,37]. It is worth stressing that the semiannihilation processes can arise if cubic terms exist among the dark matter or dark sector [34,38] when $N \geq 2$.

The complex singlet scalar models under Z_3 symmetry have been discussed a lot. For example, Refs. [39,40] study the SIMPs by introducing an extra nonzero vacuum expectation value (VEV) of the dark Higgs field with Z_3 symmetry and provide DM candidates in the mass range of $\mathcal{O}(1-100)$ MeV. Reference [41] obtains improved mass bounds by the study of Z_3 singlet dark matter with the refined unitarity bounds and treatment of early kinetic decoupling. These works indicate that two DM mass ranges, $(56.8-58.4)$ GeV $\leq m_{DM} \leq 62.8$ GeV and $m_{DM} \geq 122$ GeV, are permitted when the semiannihilation processes play an important role during the freeze-out. In this work, we focus on the study of the heavy DM case, where the annihilation of DM particles with masses larger than $\mathcal{O}(1)$ TeV occurs. On the other hand, we also consider the type-II seesaw mechanism to explain the origin of the tiny neutrino masses. We introduce an $SU(2)$ scalar triplet Δ with Z_3 charge $X_\Delta = 0$. This triplet state will obtain a small nonzero VEV after electroweak symmetry breaking (EWSB) and leads to the Majorana mass origin of neutrinos

^{*}Corresponding author.
haosun@dlut.edu.cn

Published by the American Physical Society under the terms of the Creative Commons Attribution 4.0 International license. Further distribution of this work must maintain attribution to the author(s) and the published article's title, journal citation, and DOI. Funded by SCOAP³.

through Yukawa couplings of leptons and the triplet. A further reason to consider the type-II seesaw mechanism is that the introduced triplet can play an important role in exploring the observed excess of cosmic rays observed in the electron-positron flux measured by the AMS-02 [42], Fermi-LAT [43], and DAMPE [44] experiments, arising from the leptonic decays of such a triplet during DM annihilation [45–47]. Note that the leptophilic dark matter (LDP) mechanism, in which a pair of DM particles mainly annihilate into a pair of triplets, is often adopted to fit the excess of electron-positron spectrum [45,46], where the coupling between DM and the Higgs boson is naturally negligible, leading to negligible semiannihilation effects. However, the semiannihilation effects may make sense due to the remarkable characteristics of Z_3 symmetry in our model. We therefore deliberately alleviate the LDP mechanism and reinforce the semiannihilation effects to see how they would be constrained accordingly. The W and Z boson pair from s-channel DM annihilation with subsequent decay may lead to the inappropriate antiproton spectrum measured by AMS [48] and PAMELA [49] in cosmic rays, and therefore constrains the λ_{SH} coupling between DM and the Higgs boson. It is worth stressing that the boost factor (BF) is also necessary to consider, which may come from large inhomogeneities in the dark matter distribution or due to the so-called Breit-Wigner enhancement mechanism in particle physics [50–52].

The paper is organized as follows. In Sec. II, we set up the model framework including the gauge, the Yukawa, and the scalar sectors. In Sec. III, we derive the theoretical constraints; in particular, the globality of the Z_3 symmetry vacuum is studied. In Sec. IV, we provide detailed phenomenological studies and present our numerical results. Finally, a short summary is given in Sec. V.

II. THE MODEL FRAMEWORK

We extend the SM by introducing a singlet scalar S (stabilized by a Z_3 symmetry), which can be considered the dark matter candidate. The scalar triplet Δ of hypercharge $Y = 2$ is also added to this model to generate the masses of the neutrinos. Considering that the new Z_3 symmetry keeps

the scalar potential invariant, the corresponding transformations are $H \rightarrow H$, $\Delta \rightarrow \Delta$, $S \rightarrow e^{i2\pi/3}S$. We choose the Z_3 charge of S with $X_S = 1$, and the others with Z_3 charges zero.

The total Lagrangian of the model can be written as

$$\mathcal{L}_{\text{tot}} = \mathcal{L}_{\text{Kinetic}} + \mathcal{L}_{\text{Yukawa}} - \mathcal{V}(H, \Delta, S), \quad (1)$$

with the kinetic and Yukawa terms

$$\mathcal{L}_{\text{Kinetic}} = (D^\mu H)^\dagger D_\mu H + (D^\mu \Delta)^\dagger D_\mu \Delta + (\partial^\mu S)^\dagger \partial_\mu S, \quad (2)$$

$$\mathcal{L}_{\text{Yukawa}} = \mathcal{L}_{\text{Yukawa}}^{\text{SM}} - \frac{Y_{ij}}{2} L_i^T C i \sigma_2 \Delta L_j + \text{H.c.} \quad (3)$$

Here, Y_{ij} represents the Yukawa coupling, $L_{i,j}$ are the $SU(2)_L$ doublets of left-handed leptons, i, j are the generation index, and C is the charge conjugation operator. There are no couplings between the singlet scalar S and the SM fermions. The scalar potential \mathcal{V} will be discussed in detail later. H and Δ are labels of the Higgs doublet and the triplet scalar, respectively, which are represented as

$$H = \begin{pmatrix} G^+ \\ \frac{1}{\sqrt{2}}(v_0 + h + iG^0) \end{pmatrix}, \quad (4)$$

$$\Delta = \begin{pmatrix} \frac{1}{\sqrt{2}}\delta^+ & \delta^{++} \\ \frac{1}{\sqrt{2}}(v_\Delta + \delta^0 + i\eta^0) & -\frac{1}{\sqrt{2}}\delta^+ \end{pmatrix} \quad \text{or} \quad \begin{pmatrix} \delta^{++} \\ \delta^+ \\ \frac{1}{\sqrt{2}}(v_\Delta + \delta^0 + i\eta^0) \end{pmatrix}, \quad (5)$$

where v_0 (v_Δ) is the VEV of H (Δ). G^0 , G^\pm are the Goldstone bosons that are eaten up to give mass to the SM gauge bosons.

The gauge part and Yukawa part of the model are given in Appendix A, and in this section, we focus on the scalar part of the model. The general scalar potential is given by

$$\begin{aligned} \mathcal{V}(H, \Delta, S) = & m_h^2 H^\dagger H + \lambda |H|^4 + M_\Delta^2 \text{Tr}(\Delta^\dagger \Delta) + \mu_S^2 S^\dagger S + \lambda_S (S^\dagger S)^2 + [\mu_1 (H^T i \sigma_2 \Delta^\dagger H) + \text{H.c.}] \\ & + \lambda_1 (H^\dagger H) \text{Tr}(\Delta^\dagger \Delta) + \lambda_2 (\text{Tr} \Delta^\dagger \Delta)^2 + \lambda_3 \text{Tr}(\Delta^\dagger \Delta)^2 + \lambda_4 H^\dagger \Delta \Delta^\dagger H + \lambda_{SH} |S|^2 |H|^2 \\ & + \lambda_{S\Delta} |S|^2 \text{Tr}(\Delta^\dagger \Delta) + \frac{\mu_3}{2} (S^3 + S^{\dagger 3}), \end{aligned} \quad (6)$$

which can be split into two parts:

$$\mathcal{V}(H, \Delta, S) = \mathcal{V}_{\text{nonDM}} + \mathcal{V}_{\text{DM}} \quad (7)$$

with

$$\begin{aligned} \mathcal{V}_{\text{DM}} = & \mu_S^2 S^\dagger S + \lambda_S (S^\dagger S)^2 + \lambda_{SH} |S|^2 |H|^2 \\ & + \lambda_{S\Delta} |S|^2 \text{Tr}(\Delta^\dagger \Delta) + \frac{\mu_3}{2} (S^3 + S^{\dagger 3}), \end{aligned} \quad (8)$$

where the cubic term ($S^3 + S^{\dagger 3}$) keeps Z_3 symmetry through ($S^3 + S^{\dagger 3}$) \rightarrow ($(e^{i2\pi/3}S)^3 + (e^{-i2\pi/3}S^\dagger)^3$) transformation. The parameter μ_3 can be regarded as real since its phase can be absorbed into the phase of the singlet S and not necessarily negative due to $\frac{\mu_3}{2}(S^3 + S^{\dagger 3}) \rightarrow -\frac{\mu_3}{2}((-S)^3 + (-S)^\dagger{}^3)$ changing invariance. The other parameters are also regarded as real for ignoring the CP -related issues. The SM doublet H obtains a VEV $v_0 \approx 246.22$ GeV after EWSB, and we fix the Higgs mass to be $M_h = 125$ GeV.

We summarize the key formulas we use in our model implementation as follows while recommending Ref. [53] for a more detailed description. When the doublet H and the triplet Δ get the VEVs, we obtain

$$\mathcal{V}(v_0, v_\Delta, 0) = \frac{M_h^2}{2} v_0^2 + \frac{\lambda}{4} v_0^4 + \frac{M_\Delta^2}{2} v_\Delta^2 + \frac{\lambda_1 + \lambda_4}{4} v_0^2 v_\Delta^2 + \frac{\lambda_2 + \lambda_3}{4} v_\Delta^4 - \frac{\mu_1}{\sqrt{2}} v_0^2 v_\Delta. \quad (9)$$

By solving the minimal condition of $\partial\mathcal{V}(v_0, v_\Delta, 0)/\partial v_\Delta = 0$ and $\partial\mathcal{V}(v_0, v_\Delta, 0)/\partial v_0 = 0$ under the condition $v_\Delta \ll v_0$, we can get

$$v_0 = \sqrt{\frac{-\mu^2}{\lambda}}, \quad v_\Delta \approx \frac{\mu_1 v_0^2}{\sqrt{2}(M_\Delta^2 + \frac{\lambda_1 + \lambda_4}{2} v_0^2)}. \quad (10)$$

The value of μ_1 is small in the scheme of $\mu_1 \sim v_\Delta$ so that we can neglect the associated contribution to DM annihilation. For the doubly charged scalar masses, we have

$$M_{\delta^{\pm\pm}}^2 = -v_\Delta^2 \lambda_3 - \frac{\lambda_4}{2} v_0^2 + \frac{\mu_1}{\sqrt{2}} \frac{v_0^2}{v_\Delta^2}. \quad (11)$$

Here and in the following, without confusion, we use the flavor eigenstate symbol to label its mass eigenstate. The mass squared matrix for the singly charged field can be diagonalized, with one eigenvalue zero corresponding to the charged Goldstone boson G^\pm while the other corresponds to the singly charged Higgs boson δ^\pm which can be given by

$$M_{\delta^\pm}^2 = -\frac{v_0^2 + 2v_\Delta^2}{4v_\Delta} (v_\Delta \lambda_4 - 2\sqrt{2}\mu_1). \quad (12)$$

When the neutral scalar mass matrices are diagonalized, one obtains two massive even-parity physical states h and δ^0 with the masses:

$$M_h^2 = \frac{1}{2} \left(A + B - \sqrt{(A - B)^2 + 4C^2} \right), \quad (13)$$

$$M_{\delta^0}^2 = \frac{1}{2} \left(A + B + \sqrt{(A - B)^2 + 4C^2} \right) \quad (14)$$

with

$$A = 2v_0^2 \lambda, \quad (15)$$

$$B = 2v_\Delta^2 (\lambda_2 + \lambda_3) + \frac{\mu_1}{\sqrt{2}} \frac{v_0^2}{v_\Delta}, \quad (16)$$

$$C = v_0 (v_\Delta (\lambda_1 + \lambda_4) - \sqrt{2}\mu_1). \quad (17)$$

The pseudoscalar mass matrices lead to one massless Goldstone boson G^0 and one massive physical state η^0 ,

$$M_{\eta^0}^2 = \frac{v_0^2 + 4v_\Delta^2}{\sqrt{2}v_\Delta} \mu_1. \quad (18)$$

From the relation listed above, we can write the coupling parameters as a function of the masses

$$\mu_1 = \frac{\sqrt{2}v_\Delta}{v_0^2 + 4v_\Delta^2} M_{\eta^0}^2, \quad (19)$$

$$\lambda = \frac{1}{2v_0^2} (M_h^2 \cos^2 \beta + M_{\delta^0}^2 \sin^2 \beta), \quad (20)$$

$$\lambda_4 = \frac{4}{v_0^2 + 4v_\Delta^2} M_{\eta^0}^2 - \frac{4}{v_0^2 + 2v_\Delta^2} M_{\delta^\pm}^2, \quad (21)$$

$$\lambda_3 = \frac{1}{v_\Delta^2} \left(\frac{-v_0^2}{v_0^2 + 4v_\Delta^2} M_{\eta^0}^2 + \frac{2v_0^2}{v_0^2 + 2v_\Delta^2} M_{\delta^\pm}^2 - m_{\delta^{\pm\pm}}^2 \right), \quad (22)$$

$$\lambda_2 = \frac{1}{v_\Delta^2} \left(\frac{\sin^2 \beta M_h^2 + \cos^2 \beta M_{\delta^0}^2}{2} + \frac{1}{2} \frac{v_0^2}{v_0^2 + 4v_\Delta^2} M_{\eta^0}^2 - \frac{2v_0^2}{v_0^2 + 2v_\Delta^2} M_{\delta^\pm}^2 + M_{\delta^{\pm\pm}}^2 \right), \quad (23)$$

$$\lambda_1 = -\frac{2}{v_0^2 + 4v_\Delta^2} M_{\eta^0}^2 + \frac{4}{v_0^2 + 2v_\Delta^2} M_{\delta^\pm}^2 + \frac{\sin 2\beta}{2v_0 v_\Delta} (M_h^2 - M_{\delta^0}^2) \quad (24)$$

with the mixing angle β satisfying

$$\sin(2\beta) = \frac{4v_0[-5(4M_\Delta^2 + 2(M_h^2 + M_{\delta^0}^2) + M_\Delta^2)v_\Delta^2(v_0^2 + 4v_\Delta^2) + M_\Delta^2(4v_0^4 + 6v_0^2v_\Delta^2 + 5v_\Delta^4)]}{5(M_h^2 - M_{\delta^0}^2)v_\Delta(4v_0^2 + v_\Delta^2)(v_0^2 + 4v_\Delta^2)}. \quad (25)$$

Finally, for the dark matter part, we obtain

$$M_S^2 = \mu_S^2 + \frac{\lambda_{SH}}{2} v_0^2 + \frac{\lambda_{S\Delta}}{2} v_\Delta^2. \quad (26)$$

Some other basic relations that may be useful are also listed as follows: $g = e/s_W$, $e = \sqrt{4\pi\alpha_{ew}}$, $s_W^2 = \pi\alpha_{ew}/\sqrt{2}/G_f/M_W^2$, $v_0^2 = \sqrt{1/\sqrt{2}G_f - 2v_\Delta^2}$, $M_W = \sqrt{M_Z^2/2 + \sqrt{M_Z^4/4 - M_Z^2\pi\alpha/\sqrt{2}/G_f}}$. Therefore, we choose our inputs as

$$\alpha_{ew}, M_Z, G_f, M_h \quad (27)$$

for the SM part,

$$v_\Delta, M_{\delta^{\pm\pm}}, M_{\delta^\pm}, M_{\delta^0}, M_{\eta^0} \quad (28)$$

for the triplet part, and

$$M_S, \lambda_{SH}, \lambda_{S\Delta}, \mu_3 \quad (29)$$

for the dark matter part, respectively. According to [47,54,55], for $v_\Delta \lesssim 10^{-4}$ GeV, the decays of the doubly charged Higgs boson are dominantly a same-sign dilepton. For numerical purposes, we have chosen $v_\Delta = 1$ eV satisfying the experiment constraints. However, our results are independent of the exact value of v_Δ as long as $v_\Delta \lesssim 0.1$ MeV so that the leptonic branching ratio for the Δ 's is almost 100%.

III. CONSTRAINTS

A. Perturbativity

To illustrate the theoretical bounds from the perturbativity behavior of the dimensionless scalar quartic couplings, we follow the definitions in Refs. [33,56]. As to the case of an unrotated basis, the vertices from the potential must be less than 4π to make sure that the tree-level contributions are larger than the one-loop-level quantum corrections. This condition will give the constraints on the couplings λ_i in the potential, which are

$$\begin{aligned} |6\lambda| \leq 4\pi, |\lambda_1 + \lambda_4| \leq 4\pi, |\lambda_1| \leq 4\pi, \left| \lambda_1 + \frac{\lambda_4}{2} \right| \leq 4\pi, \\ |6(\lambda_2 + \lambda_3)| \leq 4\pi, \\ |2\lambda_2| \leq 4\pi, |2(2\lambda_2 + \lambda_3)| \leq 4\pi, |\sqrt{2}\lambda_3| \leq 4\pi, |\lambda_4| \leq 4\pi, \\ |\lambda_{S\Delta}| \leq 4\pi, |\lambda_{SH}| \leq 4\pi, |4\lambda_S| \leq 4\pi. \end{aligned} \quad (30)$$

B. Perturbative unitarity

The tree-level unitarity from two-body scalar-scalar scattering processes gives another bound on the couplings λ_i in the potential. When the collision energy \sqrt{s} becomes larger, the processes will be dominated by the terms of quartic contact interaction. Although the trilinear couplings that are contributed to scattering should be included at finite collision energy [41,57], for simplicity, we only calculate the unitarity constraints with the following scenario: $s \rightarrow +\infty$. The s-wave scattering amplitudes lie in the perturbative unitarity limit, giving the constraint of the scalar-scalar scattering S -matrix values: $|\text{Re}\mathcal{M}_i| \leq \frac{1}{2}$. The perturbative unitarity in the type-II seesaw model has been studied by decomposing the matrix S by the mutually unmixed sets of channels with definite charge and CP states [53]. We extend the way of decomposing by considering the Z_3 symmetry and $X_S = 1$ singlet S introduced in our model. The matrix S can be decomposed into seven submatrix blocks structured in terms of electric charges and Z_3 charges in the initial/final states. In Appendix A, we display the initial/final states E_i and the corresponding scattering submatrix \mathcal{M}_i . The corresponding eigenvalues e_i^j of each submatrix are then calculated. The limit from perturbative unitarity on the potential's couplings λ_i , i.e., $|\text{Re}\mathcal{M}_i| \leq \frac{1}{2}$, infers $|e_i^j| \leq 8\pi$.

C. Vacuum stability

When the scalar field becomes larger in any direction of the field space, the constraint from vacuum stability is necessary since the scalar potential energy has a finite minimum. In other words, the scalar potential must have a lower bound. The quadratic and cubic terms in the scalar potential can be ignored compared with the quartic term in this limit. These constraints can be achieved by writing the matrix of the quartic interaction on the basis of non-negative field variables and ensuring that the matrix \mathcal{M} is copositive [33,58].

To parametrize the fields, we can define [33,53]

$$\begin{cases} H^\dagger H = r_1^2, \\ S = se^{i\phi}, \\ \text{Tr}(\Delta^\dagger \Delta) = r_2^2, \\ \text{Tr}(\Delta^\dagger \Delta)^2 / (\text{Tr} \Delta^\dagger \Delta)^2 \equiv n_1, & n_1 \in \left[\frac{1}{2}, 1 \right], \\ (H^\dagger \Delta \Delta^\dagger H) / (H^\dagger H \text{Tr} \Delta^\dagger \Delta) \equiv n_2, & n_2 \in [0, 1]. \end{cases} \quad (31)$$

The scalar potential related to vacuum stability can be written as

$$\begin{aligned}
\mathcal{V}(H, \Delta, S)_{\text{quartic}} &= \lambda |H|^4 + \lambda_S (S^\dagger S)^2 + \lambda_1 (H^\dagger H) \text{Tr}(\Delta^\dagger \Delta) + \lambda_2 (\text{Tr} \Delta^\dagger \Delta)^2 \\
&\quad + \lambda_3 \text{Tr}(\Delta^\dagger \Delta)^2 + \lambda_4 H^\dagger \Delta \Delta^\dagger H + \lambda_{SH} |S|^2 |H|^2 + \lambda_{S\Delta} |S|^2 \text{Tr}(\Delta^\dagger \Delta) \\
&= (r_1^2, r_2^2, s^2) \mathcal{M} \begin{pmatrix} r_1^2 \\ r_2^2 \\ s^2 \end{pmatrix},
\end{aligned} \tag{32}$$

where

$$\mathcal{M} = \begin{pmatrix} \lambda & \frac{\lambda_1 + n_2 \lambda_4}{2} & \frac{\lambda_{SH}}{2} \\ \frac{\lambda_1 + n_2 \lambda_4}{2} & \lambda_2 + \lambda_3 n_1 & \frac{\lambda_{S\Delta}}{2} \\ \frac{\lambda_{SH}}{2} & \frac{\lambda_{S\Delta}}{2} & \lambda_S \end{pmatrix} \tag{33}$$

is a 3×3 symmetric matrix. In Refs. [59,60], the necessary and sufficient conditions for the matrix \mathcal{M} to be copositive had been considered. Then, the vacuum stability conditions are given as

$$\begin{aligned}
\lambda \geq 0, \quad \lambda_2 + \lambda_3 n_1 \geq 0, \quad \lambda_S \geq 0, \quad \frac{\lambda_1 + n_2 \lambda_4}{2} + \sqrt{\lambda(\lambda_2 + \lambda_3 n_1)} \geq 0, \\
\frac{\lambda_{SH}}{2} + \sqrt{\lambda \lambda_S} \geq 0, \quad \frac{\lambda_{S\Delta}}{2} + \sqrt{(\lambda_2 + \lambda_3 n_1) \lambda_S} \geq 0, \\
\sqrt{\lambda(\lambda_2 + \lambda_3 n_1) \lambda_S} + \frac{\lambda_1 + n_2 \lambda_4}{2} \sqrt{\lambda_S} + \frac{\lambda_{SH}}{2} \sqrt{\lambda_2 + \lambda_3 n_1} + \frac{\lambda_{S\Delta}}{2} \sqrt{\lambda} \\
+ \sqrt{2 \left(\frac{\lambda_1 + n_2 \lambda_4}{2} + \sqrt{\lambda(\lambda_2 + \lambda_3 n_1)} \right) \left(\frac{\lambda_{SH}}{2} + \sqrt{\lambda \lambda_S} \right) \left(\frac{\lambda_{S\Delta}}{2} + \sqrt{(\lambda_2 + \lambda_3 n_1) \lambda_S} \right)} \geq 0.
\end{aligned} \tag{34}$$

Here, $n_1 \in [\frac{1}{2}, 1]$ and $n_2 \in [0, 1]$.

D. Globality of the Z_3 -symmetric vacuum

Since we choose the complex singlet scalar S as the DM candidate, the Z_3 symmetry should remain unbroken. The vacuum stability condition leads to the existence of a finite global minimum in the scalar potential. To ensure that the SM (EW, Z_3) vacuum is selected as the global minimum vacuum, we study the stationary points at the extreme of the scalar potential. Following the parametrization of the fields in Eq. (31), the stationary points can be obtained by taking the derivative of the potential $\mathcal{V}(r_1, r_2, s, \phi)$ concerning r_1 , r_2 , s , and ϕ , respectively, and solving the equations of

$$\begin{aligned}
0 &= r_1 (2\lambda r_1^2 + \lambda_1 r_2^2 + \lambda_4 n_2 r_2^2 + \lambda_{SH} s^2 + M_h^2), \\
0 &= r_2 (\lambda_1 r_1^2 + 2\lambda_2 r_2^2 + 2\lambda_3 n_1 r_2^2 + M_\Delta^2 + \lambda_4 n_2 r_1^2 + \lambda_{S\Delta} s^2), \\
0 &= s (4\lambda_S s^2 + 2\mu_S^2 + 2\lambda_{SH} r_1^2 + 2\lambda_{S\Delta} r_2^2 + 3\mu_3 s \cos(3\phi)), \\
0 &= s^3 \mu_3 \sin(3\phi).
\end{aligned} \tag{35}$$

Here, we have ignored μ_1 ($\mu_1 \sim \mu_\Delta$). We use Eqs. (10)–(26) to simplify the form of the solution of Eq. (35). The chosen scheme of the triplet scalar mass degeneracy leads to $\lambda_3 \simeq 0$ and $\lambda_4 \simeq 0$. On the other hand, we have $\lambda_1 \approx \lambda_2 \approx \frac{2M_h^2}{v_0^2}$ since

$v_\Delta \ll v_0$. Because of the chosen condition of $\lambda_{S\Delta} > 0$, and $M_\Delta^2 > 0$, we have $r_2 = 0$. We also set $\mu_3 \geq 0$ and $\cos 3\phi = -1$ to obtain a local minima of potential with $s \neq 0$ [38]. Finally, there are only four vacua left that should be considered. We give the discussion below.

- (1) ($r_1 = 0, s = 0$) vacuum: The EW and Z_3 symmetries remain unbroken, $v_h = v_\Delta = v_s = 0$,

$$\begin{aligned}
\mathcal{V}_{(\text{EW}, Z_3)} &= \mathcal{V}(r_1, r_2, s, \phi) \Big|_{r_1 = \frac{v_h}{\sqrt{2}}, r_2 = \frac{v_\Delta}{\sqrt{2}}, s = v_s, \phi = \frac{1}{3} \arccos(-1)} \\
&= 0.
\end{aligned} \tag{36}$$

- (2) ($r_1 \neq 0, s = 0$) vacuum: The EW symmetry is broken and Z_3 symmetry is retained with $v_h^2 \approx v_0^2$, $v_\Delta \approx 0$, $v_s = 0$,

$$\begin{aligned}
\mathcal{V}_{(\text{EW}, Z_3)} &= \mathcal{V}(r_1, r_2, s, \phi) \Big|_{r_1 = \frac{v_h}{\sqrt{2}}, r_2 = \frac{v_\Delta}{\sqrt{2}}, s = v_s, \phi = \frac{1}{3} \arccos(-1)} \\
&\approx -\frac{(M_h v_0)^2}{8}.
\end{aligned} \tag{37}$$

- (3) ($r_1 = 0, s \neq 0$) vacuum: The Z_3 symmetry is broken, and EW symmetry is retained with the condition

$$v_h = v_\Delta = 0,$$

$$v_s = \text{Root} \left[\frac{\partial \mathcal{V}(r_1, r_2, s, \phi)}{\partial s} \Big|_{r_1=0, r_2=0, \phi=\frac{1}{3}\arccos(-1)} = 0 \right]. \quad (38)$$

Here, the symbol Root denotes the solution of the partial differential equation. Thus,

$$\mathcal{V}_{(\text{EW}, \dot{Z}_3)} = \mathcal{V}(r_1, r_2, s, \phi) \Big|_{r_1=\frac{v_h}{\sqrt{2}}, r_2=\frac{v_\Delta}{\sqrt{2}}, s=v_s, \phi=\frac{1}{3}\arccos(-1)}. \quad (39)$$

- (4) ($r_1 \neq 0, s \neq 0$) vacuum: Breaking both EW and Z_3 symmetries with the condition

$$v_\Delta \approx 0,$$

$$\begin{pmatrix} v_h \\ v_s \end{pmatrix} = \text{Root} \left[\begin{pmatrix} \frac{\partial \mathcal{V}(r_1, r_2, s, \phi)}{\partial h} \Big|_{r_2=0, \phi=\frac{1}{3}\arccos(-1)} = 0 \\ \frac{\partial \mathcal{V}(r_1, r_2, s, \phi)}{\partial h=s} \Big|_{r_2=0, \phi=\frac{1}{3}\arccos(-1)} = 0 \end{pmatrix} \right]. \quad (40)$$

Thus,

$$\mathcal{V}_{(\text{EW}, \dot{Z}_3)} = \mathcal{V}(r_1, r_2, s, \phi) \Big|_{r_1=\frac{v_h}{\sqrt{2}}, r_2=\frac{v_\Delta}{\sqrt{2}}, s=v_s, \phi=\frac{1}{3}\arccos(-1)}. \quad (41)$$

To ensure the condition that the vacuum value of $\mathcal{V}_{\text{EW}, \dot{Z}_3}$ is below the others, we need to estimate the values of Eqs. (39) and (41) at given points ($M_S, \mu_3, \lambda_S, \lambda_{SH}$). We make a numerical scan in Fig. 1. First, in Fig. 1(a), we present the allowed area of λ_{SH} and $\lambda_{S\Delta}$ from perturbativity,

perturbative unitarity, and vacuum stability constraints, by taking $\lambda_3 \simeq 0, \lambda_4 \simeq 0$, and $\lambda_1 = \lambda_2 \approx \frac{2M_S^2}{v_0^2}$. The red, green, and blue areas correspond to λ_S equal to $\pi, \pi/2$, and $\pi/5$, respectively. It is clear that the constraints of λ_{SH} and $\lambda_{S\Delta}$ from these conditions are weak. Moreover, the allowed area is reduced as the value of λ_S becomes small. Then, we take the region of $\lambda_{SH}, \lambda_{S\Delta} \in [0, 4\pi]$ to scan over, and in Fig. 1(b) we present the scan result by requiring that the $\mathcal{V}_{\text{EW}, \dot{Z}_3}$ vacuum is the expected SM one. The allowed region is restricted within the $\mu_3 - M_S$ plane. One comment is that, as M_S becomes larger, the solution of the $\mathcal{V}_{\text{EW}, \dot{Z}_3}$ vacuum does not exist due to the violation of at least one of the conditions $v_s > 0, v_h^2 > 0, D_{\text{EW}, \dot{Z}_3} \geq 0$, where D_{EW, \dot{Z}_3} is the discriminant of the quadratic form defined in Ref. [38]. Only the values of $\mathcal{V}_{\text{EW}, \dot{Z}_3}$ and $\mathcal{V}_{\text{EW}, \dot{Z}_3}$ need to be compared with each other, resulting in a corresponding limit on μ_3 . This can be further seen clearly in Fig. 1(c) where we fix $M_S = 1$ TeV and vary μ_3 . The upper bounds express that the maximum value of μ_3 meets the condition of $\mathcal{V}_{\text{EW}, \dot{Z}_3} < \mathcal{V}_{\text{EW}, \dot{Z}_3}$, and the lower boundary indicates the corresponding minimum value of μ_3 . Thus, the requirement that the SM vacuum is the global minimum gives a limit on the maximum value of μ_3 . Moreover, to obtain a larger μ_3 , a larger λ_S is required.

IV. PHENOMENOLOGY

A. Relic density and direct detection constraint

We are now considering the contribution of DM thermal cross sections to the relic abundance. There are mainly three DM scatterings: (a) annihilation to the SM particles, (b) annihilation to the triplet particles, and (c) semiannihilation to a dark matter and a Higgs particle. See Fig. 2 for details of the illustrated channels.

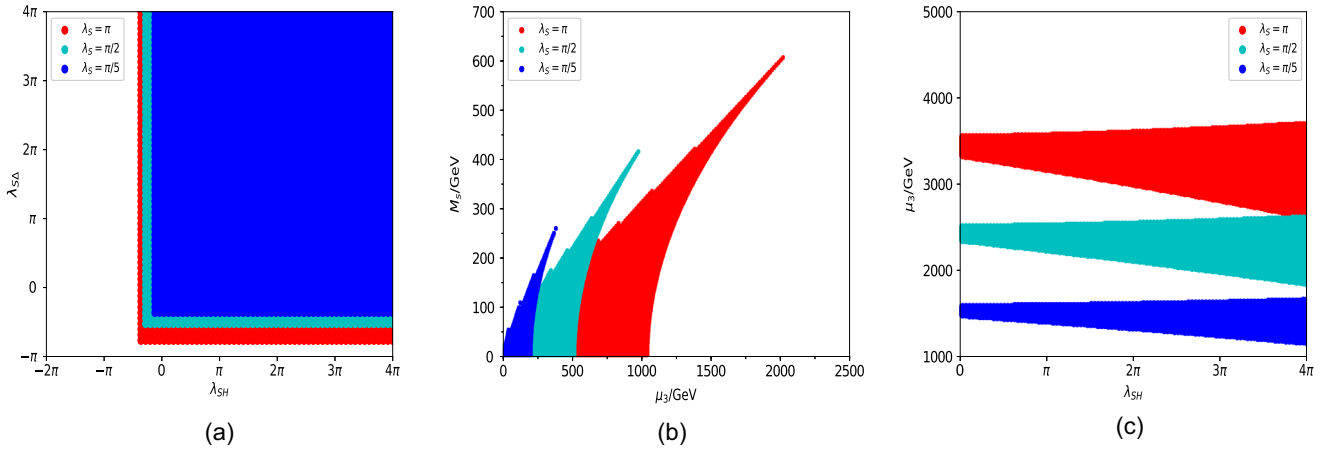


FIG. 1. (a) The possible area in the λ_{SH} vs $\lambda_{S\Delta}$ plane from perturbativity, perturbative unitarity, and vacuum stability by taking $\lambda_3 \approx \lambda_4 \approx 0$ and $\lambda_1 \approx \lambda_2 \approx \frac{2M_S^2}{v_0^2}$ at $\lambda_S = \pi, \pi/2, \pi/5$. (b) The possible area by requiring that the $\mathcal{V}_{\text{EW}, \dot{Z}_3}$ vacuum is the expected SM one. (c) The possible area in the $\lambda_{SH} - \mu_3$ plane with $M_S = 1$ TeV.

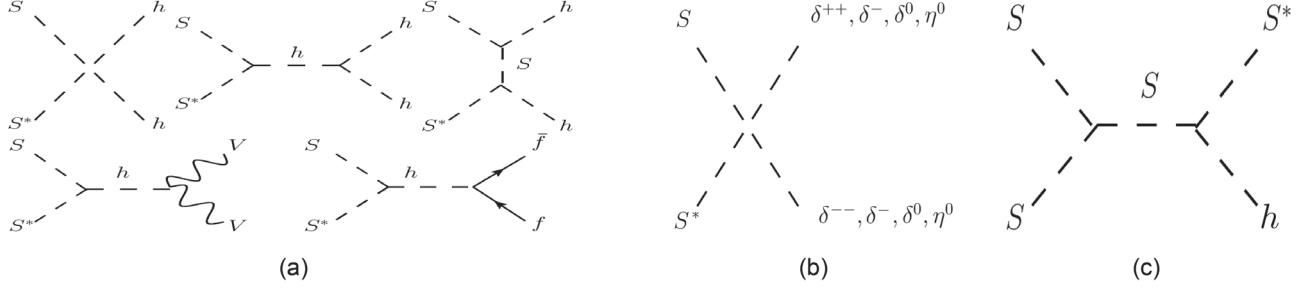


FIG. 2. DM scattering Feynman diagrams of annihilating the SM particles (a), triplet particles (b), and semiannihilating a dark matter particle and a Higgs particle (c).

The number density of the DM particle n satisfies the Boltzmann equation

$$\frac{dn}{dt} + 3Hn = -\langle\sigma v\rangle^{SS^* \rightarrow XX}(n^2 - \bar{n}^2) - \langle\sigma v\rangle^{SS^* \rightarrow \Delta\Delta}(n^2 - \bar{n}^2) - \frac{1}{2}\langle\sigma v\rangle^{SS^* \rightarrow S^*h}(n^2 - n\bar{n}), \quad (42)$$

where \bar{n} is the number density in thermal equilibrium, H is the Hubble expansion rate of the Universe, X denotes SM particles, Δ are the triplet particles ($\delta^{+(-)}$, $\delta^{+(-)}$, δ^0 , η^0), and $\langle\sigma v\rangle$ is the thermally averaged annihilation cross section, in terms of the partial wave expansion $\langle\sigma v\rangle \simeq a + bv^2$. To distinguish the different contributions of these three scattering channels on the thermal cross section, we define the scattering cross-section fraction N_i ($i = 1, 2, 3$) as

$$N_1 = \frac{\frac{1}{2}\langle v\sigma\rangle^{SS^* \rightarrow S^*h}}{\langle v\sigma\rangle^{SS^* \rightarrow \Delta\Delta} + \langle v\sigma\rangle^{SS^* \rightarrow XX} + \frac{1}{2}\langle v\sigma\rangle^{SS^* \rightarrow S^*h}} \times 100\%, \quad (43)$$

$$N_2 = \frac{\langle v\sigma\rangle^{SS^* \rightarrow \Delta\Delta}}{\langle v\sigma\rangle^{SS^* \rightarrow \Delta\Delta} + \langle v\sigma\rangle^{SS^* \rightarrow XX} + \frac{1}{2}\langle v\sigma\rangle^{SS^* \rightarrow S^*h}} \times 100\%, \quad (44)$$

$$N_3 = (1 - N_1 - N_2). \quad (45)$$

Here, N_3 denotes the fraction of DM pairs annihilating to SM particles. To calculate the DM relic density and the fraction N_i we use the micrOMEGAS5.0.6 package [61], in which the model has been implemented through the FeynRules package [62]. To constrain the parameter space, we require the relic density to fit the 2σ C.L. range of the Planck result [63]: $\Omega_{\text{DM}}h^2 = 0.1199 \pm 0.0027$. The direct detection constraint is obtained from the spin-independent (SI) elastic scattering measurements, which can be given by [46]

$$\sigma_{\text{SI}} = \frac{\lambda_{SH}^2}{\pi M_h^4} \frac{M_N^2}{(M_N + M_S)^2} \times 0.0706 M_N^2, \quad (46)$$

where the nucleon mass $M_N \simeq 0.939$ GeV. The PandaX-4T experiment [64] has given the best upper limit of the SI elastic scattering cross section at a given DM mass M_S , which will lead to a maximum value of λ_{SH} . As N_1 is proportional to $\mu_3^2 \lambda_{SH}^2 / M_S^6$, in order to enhance the semiannihilation contribution characterized by the Z_3 singlet scalar S , we choose $\lambda_S = \pi$ so that the parameter μ_3 is as large as possible, while the condition that the (EW, Z_3) vacuum being the global minimum is still guaranteed; see Fig. 1(c) for a discussion.

A detailed scan is shown in Fig. 3. As can be seen, we fix $M_\Delta = 0.9$ TeV while varying the benchmark values of M_S that obey $M_S > M_\Delta$. Meanwhile, adopting the requirement that the relic density should fit the Planck measurement in the 2σ C.L. range, the parameter space of λ_{SH} vs $\lambda_{S\Delta}$ is constrained within a quarter circle ring. Different rings relate to different choices of M_S . The vertical lines

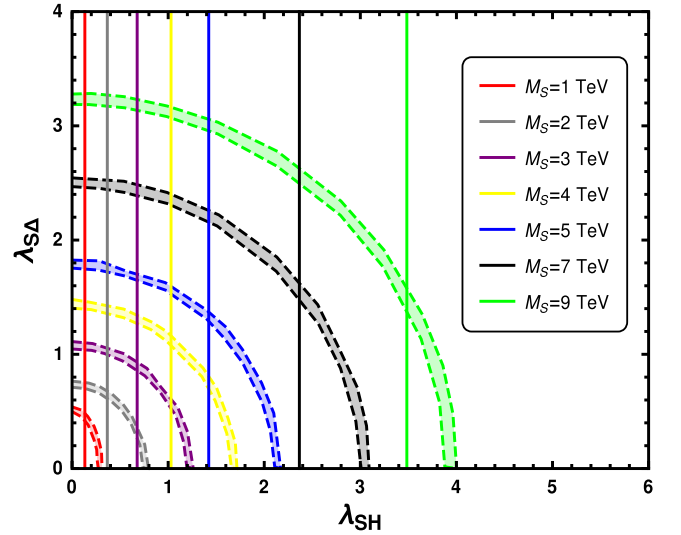


FIG. 3. The allowed parameter space in the λ_{SH} vs $\lambda_{S\Delta}$ plane adopts the requirement that the relic density should fit the Planck measurement in the 2σ C.L. range. The vertical line is the upper value of λ_{SH} at a given M_S based on PandaX-4T measurements.

correspond to the upper values of λ_{SH} at a given M_S based on the PandaX-4T measurements. Clearly, as the DM mass M_S becomes larger, the upper boundary of λ_{SH} becomes larger correspondingly. The crossover point (or precisely, segment) of the same colored ring and line relates to a boundary point. The region on the left side of the point fits both Planck as well as PandaX-4T measurements, while the right side does not fit that of PandaX-4T. With the increase of DM mass, the restriction of the Planck experiment on λ_{SH} is more important than that of PandaX-4T.

B. Antiproton spectrum and electron-positron flux

The DM particles may annihilate to W and Z boson pairs through the s-channel Higgs exchange. The subsequent decays of the bosons to antiprotons will be responsible for the interpretation of the cosmic-ray antiprotons spectrum that has been measured by the AMS [48] and PAMELA [49] Collaborations. On the other hand, the triplets produced from DM (co)annihilation may decay to leptons ($\Delta \rightarrow \ell^i \ell^j$) through Yukawa interactions, and it is therefore possible to account for the excess of electron-positron flux in cosmic rays exhibited in the AMS-02, Fermi-LAT, and DAMPE experiments [42–44]. Notice the excess of positron-electron flux in cosmic rays may also be explained by astrophysical evidence, for example, an isolated young pulsar [65]. Here in our paper, we focus on the DM interpretation, although it is possible that the cosmic-ray fluxes are not due to DM but due to mundane astrophysics. Interpretation of the cosmic-ray excesses by the dark matter has been discussed a lot, and related works can be found in Refs. [47,66–75]. We choose the DM mass at the 2 TeV scale, $M_\Delta = 0.9$ TeV and $\mu_3 \approx 10$ TeV, and the last value is chosen to enhance the semiannihilation as much as possible. We focus on the parameter space where our model can give a natural DM explanation of both cosmic-ray measurements as well as fitting the relic density measurement simultaneously, which also includes semiannihilation effects.

To calculate the antiproton flux and electron-positron flux, we use the following parametrization functions [76–78]:

$$\log_{10} \Phi_{\bar{p}}^{\text{bkg}} = -1.64 + 0.07x - x^2 - 0.02x^3 + 0.028x^4, \quad (47)$$

$$\Phi_{e^-}^{\text{prim}}(E) = \frac{0.16E^{-1.1}}{1 + 11E^{0.9} + 3.2E^{2.15}} [\text{GeV}^{-1} \text{cm}^{-2} \text{s}^{-1} \text{sr}^{-1}], \quad (48)$$

$$\Phi_{e^\pm}^{\text{sec}}(E) = \frac{0.70E^{0.7}}{1 + 110E^{1.5} + 600E^{2.9} + 580E^{4.2}} \times [\text{GeV}^{-1} \text{cm}^{-2} \text{s}^{-1} \text{sr}^{-1}], \quad (49)$$

$$\Phi_{e^+}^{\text{sec}}(E) = \frac{4.5E^{0.7}}{1 + 650E^{2.3} + 1500E^{4.2}} [\text{GeV}^{-1} \text{cm}^{-2} \text{s}^{-1} \text{sr}^{-1}], \quad (50)$$

with $x = \log_{10} T/\text{GeV}$ in Eq. (47), and the label $\Phi_{\bar{p}}^{\text{bkg}}$ denotes the cosmic-ray antiproton background. The label $\Phi^{\text{prim(sec)}}$ in Eqs. (48)–(50) means the primary (secondary) cosmic ray of the electron or positron background. The formula is appropriate for the energy range 10–1000 GeV [77]. The primary and secondary electron backgrounds are originated from supernova remnants and cosmic-ray spallation in the interstellar medium, respectively. The secondary positron background comes from primary protons colliding with other nuclei in the interstellar medium. With the value of BF mentioned above, the total antiproton, positron plus electron flux, and positron flux are given by

$$\Phi_{\bar{p}} = \Phi_{\bar{p}}^{\text{bkg}} + BF \times \Phi_{\bar{p}}^{\text{DM}}, \quad (51)$$

$$\Phi_{e^+} + \Phi_{e^-} = k(\Phi_{e^-}^{\text{prim}} + \Phi_{e^-}^{\text{sec}} + \Phi_{e^+}^{\text{sec}}) + BF \times (\Phi_{e^-}^{\text{DM}} + \Phi_{e^+}^{\text{DM}}), \quad (52)$$

$$\Phi_{e^+} = k\Phi_{e^+}^{\text{sec}} + BF \times \Phi_{e^+}^{\text{DM}}, \quad (53)$$

where Φ^{DM} is the corresponding flux from DM pair annihilation. According to [45,77,79], we have considered the normalization of the primary electron flux to be undetermined and parametrized by the parameter of k . According to [45], the total positron fraction and the total electron + positron flux are required to be consistent with the updated AMS-02 results, and this requirement in the model favors the values of k in the range 0.8–0.9. In our work, we use $k = 0.9$ to fit the experimental data. The background fluxes can, in principle, be estimated. To calculate Φ^{DM} we use micrOMEGAS, in which the density distribution of DM in the Galactic halo is taken from Navarro-Frenk-White density, and the effects of galactic-charged-particle propagation and solar modulation are considered.

The obtained cosmic ray fluxes as well as the experimental data points are put into a composite χ^2 function which is defined as

$$\chi^2 = \sum_i \frac{(f_i^{\text{th}} - f_i^{\text{exp}})^2}{\sigma_i^2}, \quad (54)$$

where the f_i 's are the relevant observables, and in our work is a positron fraction. δf_i are the experimental errors (stat + syst) obtained from [80]. We take AMS-02 data points for $E > 15$ GeV in our χ^2 analysis with 36 points in total. It is worth stressing that we can have a poor fit when we include the low-energy data points below 15 GeV, but

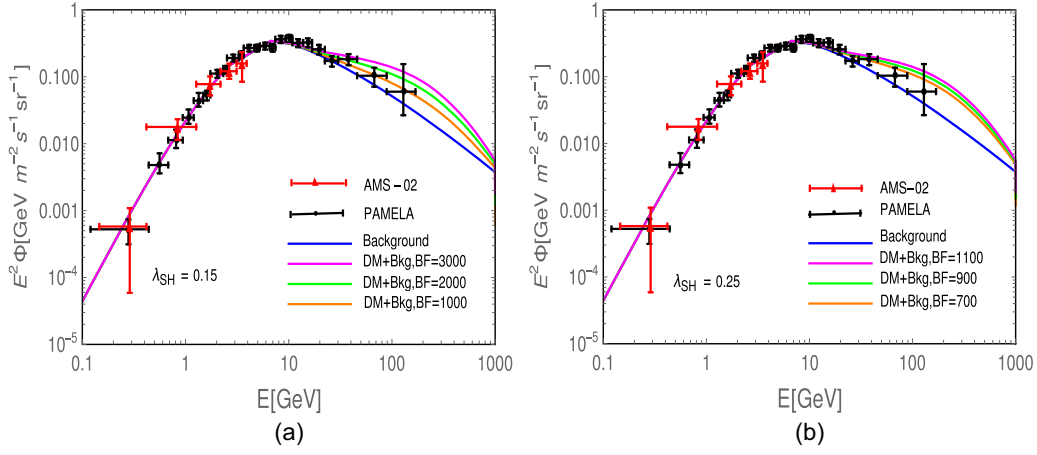


FIG. 4. Background and background + DM (Bkg + DM) of the cosmic-ray antiproton flux, where we choose $\lambda_{SH} = 0.15$ in (a) and $\lambda_{SH} = 0.25$ in (b). The data points in both figures label the PAMELA [49] and AMS [48] measurements.

we note that such discrepancies for $E < 15$ GeV can be accounted for by uncertainties caused by solar modulation [81] as well as background flux uncertainties according to [45]. On the other hand, we do not use any other previous datasets for positron fraction such as Fermi-LAT, because AMS-02 data are much more precious.

Considering the difference in the electron-positron spectrum between the DAMPE and Fermi-LAT measurements when $E > 1$ TeV, we focus on the calculation of the flux when the value of E is located in the range of 0–1000 GeV. The results of the cosmic-ray antiproton are displayed in Fig. 4 with different values of the BF taken as a free parameter. Figure 4(a) displays the background and Bkg + DM for $\Phi_{\bar{p}}$ in the case of $\lambda_{SH} = 0.15$, while Fig. 4(b) gives the results in the case of $\lambda_{SH} = 0.25$. As can be seen in Fig. 4(a), at a given value of $\lambda_{SH} = 0.15$, the PAMELA [49] results impose strong restrictions on the BF, where the maximum value is about 2000, while for $\lambda_{SH} = 0.25$, the allowed BF is about 700.

In Figs. 5 and 7, we give the results of the background and Bkg + DM of cosmic-ray positron-electron fluxes with $\lambda_{SH} = 0.15$, as well as $\lambda_{SH} = 0.25$ in both the inverted hierarchy (IH) [Figs. 5(a) and 7(a)] and normal hierarchy (NH) [Figs. 5(b) and 7(b)] scenarios, respectively. We give the corresponding results of the comparison of the positron fraction observed by the AMS-02 in Figs. 6 ($\lambda_{SH} = 0.15$) and 8 ($\lambda_{SH} = 0.25$), which is defined by $\Phi_{e^+}/(\Phi_{e^+} + \Phi_{e^-})$. For $\lambda_{SH} = 0.15$, according to the results of the positron-electron fluxes with the DAMPE, Fermi-LAT, and AMS-02 experiments, we find that the flux with the small BF can meet the AMS and PAMELA results, while the DAMPE and Fermi-LAT experiments favor large values of the BF. For a given DM mass, the positron-electron flux for the NH scenario is softer toward the higher-energy end as compared to that for the IH scenario in our model. On the other hand, according to the results of the comparison of the positron fraction observed by AMS-02, the NH scenario is different from the IH scenario, as we can see that there

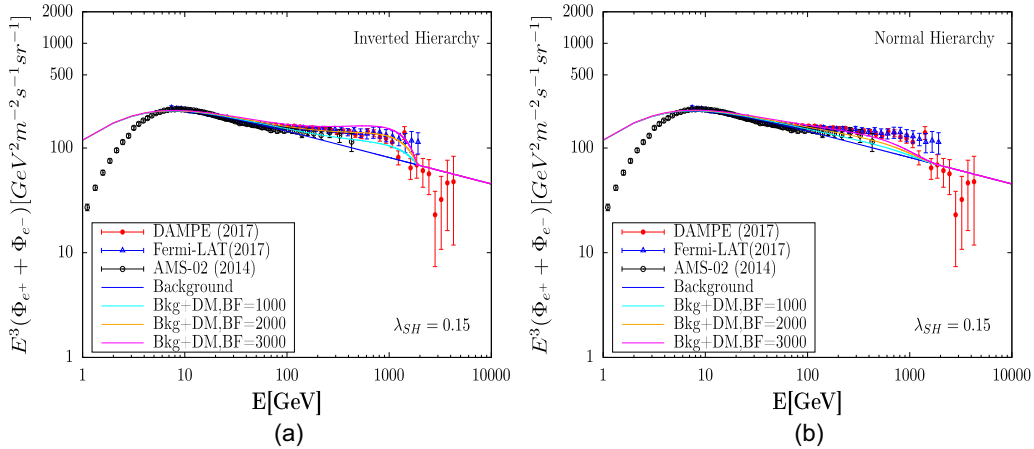


FIG. 5. Background and Bkg + DM of cosmic-ray positron-electron fluxes in the case of $\lambda_{SH} = 0.15$, where (a) corresponds to the IH scenario and (b) is the NH scenario. The data points in both figures stand for the AMS-02 [42], Fermi-LAT [43], and DAMPE [44] measurements.

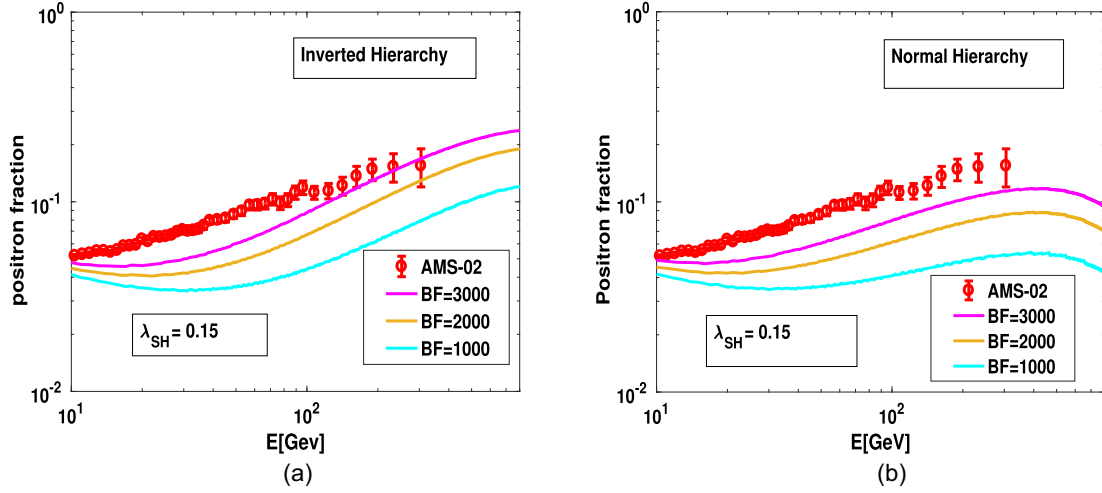


FIG. 6. Comparison of the positron fraction observed by AMS-02 [42] (the red points) in the case of $\lambda_{SH} = 0.15$ with the BF varying from 1000 to 3000, where (a) corresponds to the IH scenario and (b) is the NH scenario.

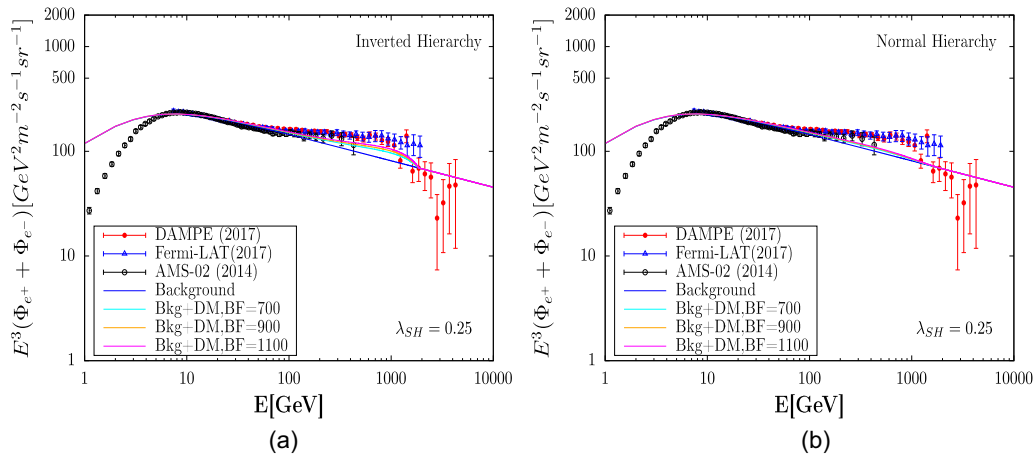


FIG. 7. Same as Fig. 5 but with $\lambda_{SH} = 0.25$.

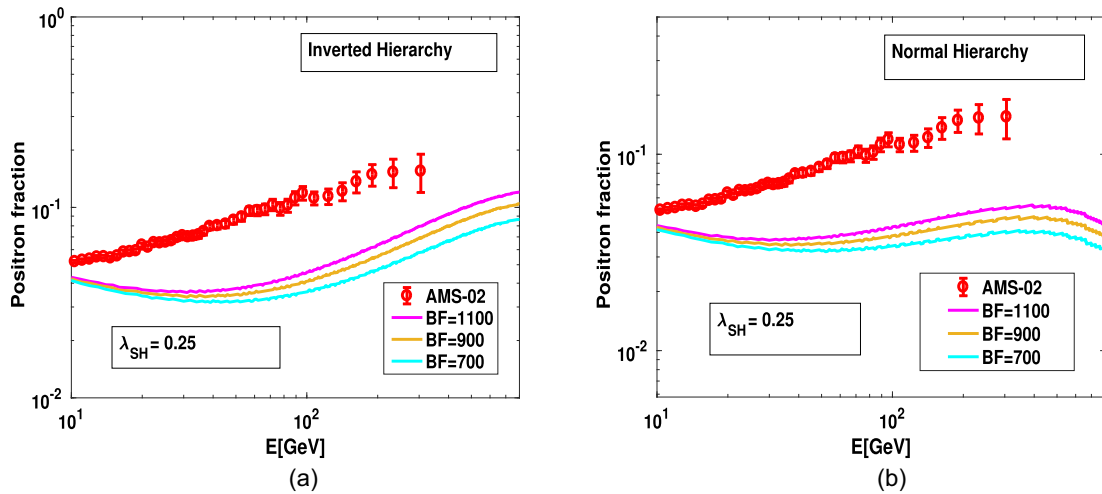


FIG. 8. Same as Fig. 6 but with $\lambda_{SH} = 0.25$.

displays a suppression in the high E region for the NH case. The differences in behavior between these two scenarios can be understood as that, in our model, DM particles mainly annihilate into electron final states in the IH scenario and tau final states in the NH scenario instead, which can be seen directly from the final state decay fraction in Table III, which is $e:\mu:\tau \approx 1:0.2:0.3$ for the IH scenario and $e:\mu:\tau \approx 1:0.5:1.4$ for that of the NH scenario. If the triplets decay mainly into electron/positron final states, the positron flux arising from DM annihilation will rise sharply above the background as long as we go to higher energies and will eventually drop to the background level before $E = M_S$, while for the NH scenario, the triplets mostly decay into taus and subsequently decay to electrons, and one can obtain a much softer energy spectrum of the positron flux before eventually dropping to the background level at some $E < M_S$.

We present a similar sector in Figs. 7 and 8, and the only difference is $\lambda_{SH} = 0.25$. From Fig. 4(b), we know that the maximum value BF is restricted to less than about 700, otherwise it may lead to an inappropriate antiproton spectrum measured by PAMELA. Compared with the observed positron-electron flux, we find that the IH scenario can meet the Fermi-LAT measurements and the AMS-02 experiment, but the NH scenario can only meet the AMS-02 experiment. However, both IH and NH scenarios cannot meet the observed positron fraction from the AMS-02 experiment, even much lower than the current results. We note that λ_{SH} should not be much higher. In fact, the larger λ_{SH} is excluded by the AMS and PAMELA experiments, as in this case, the triplet scalar productions are gradually reduced.

We also select some feature points that meet the requirement of the relic density, direct detection constraints, and antiproton flux exhibited by AMS and PAMELA experimental results in Table I. The fraction scattering cross-section N_i and the maximum value of the BF that is

TABLE I. The fraction scattering cross-section N_i and maximum value of BFs at different values of $\lambda_{SH}/\lambda_{S\Delta}$.

λ_{SH}	0.15	0.2	0.25	0.3	0.35
$\lambda_{S\Delta}$	0.73	0.71	0.69	0.67	0.64
N1 (%)	2	4	6	8	11
N2 (%)	96	90	86	84	72
BF	$\lesssim 2000$	$\lesssim 1300$	$\lesssim 700$	$\lesssim 500$	$\lesssim 400$

TABLE II. The best-fit values of the BF along with the corresponding χ^2 for a χ^2 analysis of the AMS-02 positron fraction, where we fix $\lambda_{SH} = 0.1$ and $\lambda_{S\Delta} = 0.74$.

	BF	χ^2_{\min}
IH	5813	111.013
NH	5417	19.9291

allowable are shown, corresponding to different values of $\lambda_{SH}/\lambda_{S\Delta}$. We see that each value of λ_{SH} has an upper limit on the BF. As λ_{SH} becomes larger, the BF value is reduced correspondingly, while the semiannihilation contribution enhances, though it only stands for a small fraction of the total. In addition, small values of the BF and $\lambda_{S\Delta}$ will also lead to a bad fit to the DAMPE and Fermi-LAT measurements. After the detailed analysis above, we conclude that to meet the appropriate antiproton spectrum and electron-positron flux, especially for DAMPE and Fermi-LAT, we demand that the λ_{SH} value should not be large, i.e., smaller than 0.35. As a result, the fraction of the semiannihilation cross section is less than 11%.

To summarize, we give the best-fit values of the BF along with the corresponding χ^2 for a χ^2 analysis of AMS-02 positron fraction in Table II, where we fix $\lambda_{SH} = 0.1$ and $\lambda_{S\Delta} = 0.74$. In addition, we give the results of the background and Bkg + DM of cosmic-ray electron-positron flux in Fig. 9(a) and a comparison of the positron fraction observed by AMS-02 in Fig. 9(b) with the IH scenario as

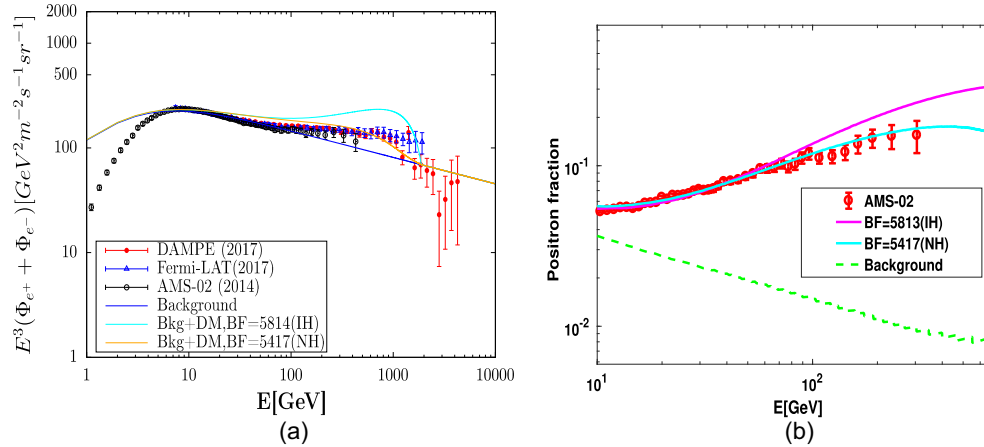


FIG. 9. Background and Bkg + DM of cosmic-ray electron-positron flux in (a) and comparison of the positron fraction observed by AMS-02 [42] in (b) with the IH scenario as well as NH scenario. The data points in (a) stand for the AMS-02 [42], Fermi-LAT [43], and DAMPE [44] measurements, and the data points in (b) stand for the AMS-02 [42].

well as NH scenario. It is obvious that the NH scenario can give a better fit with the AMS-02 and DAMPE experiment compared with the IH scenario. As we mentioned above, the positron energy spectrum is softer in the NH case, as it comes from muon and tau decays, while for the IH scenario, the spectrum is harder because it comes directly from the Δ decay. Since the rise in the AMS-02 positron fraction becomes softer toward higher energies, it is easier to fit both low- and high-energy bins for the NH case compared to the IH case.

V. SUMMARY

The idea of relating a singlet scalar with Z_2 symmetry to the type-II seesaw mechanism has been extensively studied in the literature, for example, Refs. [45,82]. In this paper, we combine the type-II seesaw mechanism with a complex singlet scalar of Z_3 symmetry to solve the origin of neutrino mass and dark matter beyond the SM in one framework. The new cubic term $S^3 + S^{\dagger 3}$ results in semiannihilation effects contributing to Ωh^2 . We consider the dark matter in the heavy mass region ($M_S > M_\Delta$) and degenerate triplet scalar masses for numerical analysis. We find that the constraints from perturbativity, perturbative unitarity, and vacuum stability on λ_{SH} and $\lambda_{S\Delta}$ are weak. The requirement that the $\mathcal{V}_{(\text{EW}, Z_3)}$ vacuum is the global minimum, or precisely, $\mathcal{V}_{(\text{EW}, Z_3)} < \mathcal{V}_{(\text{EW}, \mathbb{Z}_3)}$, gives μ_3 a maximum value, which leads to the fact that the semiannihilation process contribution fraction (N_1) has an upper limit. We calculate the viable areas of λ_{SH} and $\lambda_{S\Delta}$ which are consistent with the Planck and PandaX-4T measurements at given values of M_Δ and M_S . As the dark mass M_S increases, the semiannihilation process contribution fraction N_1 decreases gradually at the permitted maximum value of λ_{SH} and μ_3 .

When the triplets and the W, Z boson pairs are produced from DM (co)annihilation, they will be responsible for the interpretation of the excess of electron-positron flux and antiproton spectrum with their subsequent decays. We alleviate the leptophilic properties of the DM to enhance the semiannihilation effects and calculate those fluxes in both NH and IH scenarios. We find that fitting the antiproton spectrum measured by AMS and PAMELA shows that the maximum value of the BF decreases with the increase of λ_{SH} , and to fit the DAMPE and Fermi-LAT measurements one requires a large BF and small λ_{SH} . To fit simultaneously the electron-positron flux as well as the antiproton spectrum, a strong restriction is set on the semiannihilation cross-section fraction (N_1); for example, for $M_S = 2$ TeV, N_1 should be less than 11%. In either case, the NH scenario is always the favored one. We note that the model requires a large BF of order 10^3 – 10^4 in the DM annihilation rate to explain the observed e^+/e^- excess. According to [45], such a large BF can still be consistent with the indirect detection of experimental limits of neutrino and gamma-ray fluxes [83] as well as the

observable effects in the big bang nucleosynthesis and cosmic microwave background precision measurements.

ACKNOWLEDGMENTS

The authors would like to thank Zhi-Long Han, Chuan-Hung Chen, and Takaaki Nomura for their useful and kind help during technological implementation. H. S. is supported by the National Natural Science Foundation of China (Grants No. 12075043 and No. 12147205).

APPENDIX A: RELATED LAGRANGIAN

1. The gauge part

In Eq. (2), the covariant derivative can be expressed as

$$D_\mu = \partial_\mu + i \frac{g}{\sqrt{2}} (T^+ W_\mu^+ + T^- W_\mu^-) + i \frac{g}{c_W} (T^3 - s_W^2 Q) Z_\mu + i e Q A_\mu, \quad (\text{A1})$$

where W_μ^\pm , Z_μ , and A_μ are the SM gauge bosons, g is the gauge coupling of $SU(2)_L$, and θ_W stands for the Weinberg angle with $s_W(c_W) = \sin \theta_W(\cos \theta_W)$ for short. Q is the charge operator. For the scalar doublet, T is associated with the Pauli matrices by

$$T^\pm = \frac{1}{2}(\sigma_1 \pm \sigma_2), \quad T^3 = \sigma_3, \quad (\text{A2})$$

and $Q = \text{diag}(1, 0)$, while for the scalar triplet, we have $Q = \text{diag}(2, 1, 0)$ and $T^\pm = T^1 \pm iT^2$ with the $SU(2)_L$ generators chosen as

$$T^1 = \frac{1}{\sqrt{2}} \begin{pmatrix} 0 & 1 & 0 \\ 1 & 0 & 1 \\ 0 & 1 & 0 \end{pmatrix}, \quad T^2 = \frac{1}{\sqrt{2}} \begin{pmatrix} 0 & -i & 0 \\ i & 0 & -i \\ 0 & i & 0 \end{pmatrix}, \quad (\text{A3})$$

$$T^3 = \begin{pmatrix} 1 & 0 & 0 \\ 0 & 0 & 0 \\ 0 & 0 & -1 \end{pmatrix}.$$

The kinetic terms of the triplet Δ will change the SM W^\pm and Z gauge boson masses, which can be expressed after spontaneous symmetry breaking as

$$m_W^2 = \frac{g^2 v_0^2}{4} \left(1 + \frac{2v_\Delta^2}{v_0^2} \right), \quad m_Z^2 = \frac{g^2 v_0^2}{4c_W^2} \left(1 + \frac{4v_\Delta^2}{v_0^2} \right), \quad (\text{A4})$$

and therefore affect the SM ρ parameter at the tree level

$$\rho = \frac{m_W^2}{m_Z^2 c_W^2} = \frac{1 + 2v_\Delta^2/v_0^2}{1 + 4v_\Delta^2/v_0^2}. \quad (\text{A5})$$

The current electroweak precision data constraints require the ρ parameter to be $1.0004_{-0.0004}^{+0.0003}$ [84] and thus give

$$\frac{v_\Delta}{v_0} \lesssim 0.02 \quad \text{or} \quad v_\Delta \lesssim 5 \text{ GeV}. \quad (\text{A6})$$

One can find that the gauge interactions of the triplet particles such as the $\delta^0 W^+ W^-$ and $\delta^0 Z Z$ vertexes are all proportional to v_Δ . A more detailed discussion can be found in Ref. [85]. Since in our case we consider the singlet scalar, there is no direct connection between S and the gauge fields.

2. The Yukawa part

The triplet scalar couplings with the leptons through the type-II seesaw mechanism are given, in terms of Yukawa matrix \mathbf{Y} , by

$$\mathcal{L}_{\text{Yukawa}}^{\text{New}} = -\frac{1}{2} L^T C \mathbf{Y} i \sigma_2 \Delta L + \text{H.c.}, \quad (\text{A7})$$

with $C = i\gamma_0 \gamma_2$. $L^T = (\nu_\ell^T, \ell^T)$ is the transpose of the $SU(2)_L$ left-handed lepton doublet mentioned above. We

can simply obtain the expanded expression

$$\begin{aligned} \mathcal{L}_{\text{Yukawa}}^{\text{New}} = & -\frac{Y_{ij}}{2} \nu_i^T C \nu_j \frac{v_\Delta + \delta^0 + i\eta^0}{\sqrt{2}} + Y_{ij} \nu_i^T C \ell_j \frac{\delta^+}{\sqrt{2}} \\ & + \frac{Y_{ij}}{2} \ell_i^T C \ell_j \delta^{++} + \text{H.c.}, \end{aligned} \quad (\text{A8})$$

with $i, j = 1, 2, 3$. Therefore, \mathbf{Y} is related to the Majorana neutrino mass matrix in flavor eigenstates by $\mathbf{m}_\nu = v_\Delta \mathbf{Y} / \sqrt{2}$. Assume that the physical neutrino mass matrix is $\mathbf{m}_\nu^{\text{diag}} = \text{diag}(m_1, m_2, m_3)$, with the help of Pontecorvo-Maki-Nakagawa-Sakata (PMNS) matrix U_{PMNS} , the Yukawa matrix can thus be written as

$$\mathbf{Y} = \frac{\sqrt{2}}{v_\Delta} U_{\text{PMNS}}^* \mathbf{m}_\nu^{\text{diag}} U_{\text{PMNS}}^\dagger = \frac{\sqrt{2}}{v_\Delta} \begin{pmatrix} m_{ee} & m_{e\mu} & m_{e\tau} \\ m_{e\mu} & m_{\mu\mu} & m_{\mu\tau} \\ m_{e\tau} & m_{\mu\tau} & m_{\tau\tau} \end{pmatrix}. \quad (\text{A9})$$

The U_{PMNS} matrix can be parametrized by

$$U_{\text{PMNS}} = \begin{pmatrix} c_{12}c_{13} & c_{13}s_{12} & e^{-i\delta}s_{13} \\ -c_{12}s_{13}s_{23}e^{i\delta} - c_{23}s_{12} & c_{12}c_{23} - e^{i\delta}s_{12}s_{13}s_{23} & c_{13}s_{23} \\ s_{12}s_{23} - e^{i\delta}c_{12}c_{23}s_{13} & -c_{23}s_{12}s_{13}e^{i\delta} - c_{12}s_{23} & c_{13}c_{23} \end{pmatrix} \text{diag}(e^{i\Phi_1/2}, 1, e^{i\Phi_2/2}) \quad (\text{A10})$$

with $s_{ij} = \sin \theta_{ij}$, $c_{ij} = \cos \theta_{ij}$, and δ, Φ_i are the Dirac and Majorana CP phases, respectively. For illustration purposes, we set the two Majorana phases and the lightest neutrino mass to be zero and the masses obey

- (i) the NH scenario ($m_1 < m_2 < m_3$) with $m_2 = (m_1^2 + \Delta m_{21}^2)^{1/2}$, $m_3 = (m_1^2 + \Delta m_{31}^2)^{1/2}$, and
- (ii) the IH scenario ($m_3 < m_1 < m_2$) with $m_1 = (m_3^2 + \Delta m_{31}^2)^{1/2}$, $m_2 = (m_1^2 + \Delta m_{21}^2)^{1/2}$,

where $\Delta m_{ij}^2 = m_j^2 - m_i^2$. Using the central values of the global analysis based on the neutrino oscillation data [86]

$$\begin{aligned} \Delta m_{21}^2 &= 7.50 \times 10^{-5} \text{ eV}^2, & |\Delta m_{31}^2| &= 2.524(2.514) \times 10^{-3} \text{ eV}^2, \\ \sin^2 \theta_{12} &= 0.306, & \sin^2 \theta_{23} &= 0.441(0.587), \\ \delta &= 261^\circ(277^\circ), & \sin^2 \theta_{13} &= 0.02166(0.02179), \end{aligned} \quad (\text{A11})$$

where the values in parentheses correspond to the IH scenario, and we obtain the Yukawa coupling matrix

$$\mathbf{Y}^{\text{NH}} = \frac{10^{-2} \text{ eV}}{v_\Delta} \times \begin{pmatrix} 0.1558 + 0.0336i & 0.2232 - 0.5050i & -0.3432 - 0.5686i \\ 0.2232 - 0.5050i & 2.5103 - 0.0584i & 1.0963 - 0.03901i \\ 2.1403 - 0.0078i & 1.0963 - 0.0390i & 3.0004 + 0.0566i \end{pmatrix} \quad (\text{A12})$$

and

$$\mathbf{Y}^{\text{IH}} = \frac{10^{-2} \text{ eV}}{v_\Delta} \times \begin{pmatrix} 3.6631 & -1.2660 - 0.4156i & 1.4057 - 0.3487i \\ -1.2660 - 0.4158i & 0.8693 + 0.2874i & -1.0963 - 0.03901i \\ 1.4057 - 0.3487i & -1.0963 - 0.03901i & 1.1869 - 0.2676i \end{pmatrix}. \quad (\text{A13})$$

With the help of these known Yukawa coupling values, the branching ratios of the triplet scalars can be calculated and listed in Table III for both the IH and NH scenarios. The decay of the $\delta^{\pm\pm}$ final states produces a fraction of $e:\mu:\tau \approx 1:0.2:0.3$

TABLE III. Branching ratios (Br) of triplet scalars decay calculated by CalcHEP [87] in the NH and IH scenarios, with the corresponding Yukawa coupling values listed in Eqs. (A12) and (A13).

$\delta^{\pm\pm}$	IH (%)	NH (%)	δ^0/η^0	IH (%)	NH (%)	δ^\pm	IH (%)	NH (%)
$\text{Br}(e^\pm e^\pm)$	51.80	1.32	$\text{Br}(\nu_e \nu_e)$	51.80	1.32	$\text{Br}(e^\pm \nu_e)$	51.80	1.32
$\text{Br}(\mu^\pm \mu^\pm)$	3.24	3.28	$\text{Br}(\nu_\mu \nu_\mu)$	3.24	3.28	$\text{Br}(e^\pm \nu_\mu)$	6.86	1.58
$\text{Br}(\tau^\pm \tau^\pm)$	5.72	4.68	$\text{Br}(\nu_\tau \nu_\tau)$	5.72	4.68	$\text{Br}(e^\pm \nu_\tau)$	8.10	22.9
$\text{Br}(e^\pm \mu^\pm)$	13.70	31.7	$\text{Br}(\nu_e \nu_\mu)$	13.70	31.7	$\text{Br}(\mu^\pm \nu_e)$	6.86	1.58
$\text{Br}(e^\pm \tau^\pm)$	16.20	45.9	$\text{Br}(\nu_e \nu_\tau)$	16.20	45.9	$\text{Br}(\mu^\pm \nu_\mu)$	3.24	3.28
$\text{Br}(\mu^\pm \tau^\pm)$	9.30	1.25	$\text{Br}(\nu_\mu \nu_\tau)$	9.30	1.25	$\text{Br}(\mu^\pm \nu_\tau)$	4.65	6.26
						$\text{Br}(\tau^\pm \nu_e)$	8.10	22.9
						$\text{Br}(\tau^\pm \nu_\mu)$	4.65	62.6
						$\text{Br}(\tau^\pm \nu_\tau)$	5.72	4.68

and 1:0.5:1.4 in the IH and NH scenarios, respectively. The electron-rich final states in the IH case point to the excess of the spectrum indicated by the AMS-02, DAMPE, and Fermi-LAT measurements. We will give a more detailed discussion in Appendix B.

The singly and doubly charged scalars in the type-II seesaw model also contribute to the lepton flavor violating processes, and therefore put the stringent lower bounds based on the current experiment [88,89] given $v_\Delta \cdot M_\Delta \geq 150$ eV GeV, where M_Δ is the triplet mass. The limits from the LHC direct searches for doubly charged Higgs bosons also require $M_\Delta \gtrsim 770\text{--}870$ GeV [90,91].

APPENDIX B: FORMULAS

The first submatrix \mathcal{M}_1 of the scattering whose initial and final states have charge zero is $E_1 = (G^+ \delta^-, \delta^+ G^-, h\eta^0, \delta^0 G^0, G^0 \eta^0, h\delta^0, h s, \delta^0 S, G^0 S, \eta^0 S, h S^*, \delta^0 S^*, G^0 S^*, \eta^0 S^*)$. The first six states have discrete Z_3 symmetry with charge $X = 0$, and the last eight states have $X = 2$. One can find

$$\mathcal{M}_1 = \begin{pmatrix} \lambda_1 + \frac{\lambda_4}{2} & 0 & \frac{i\lambda_4}{2\sqrt{2}} & -\frac{i\lambda_4}{2\sqrt{2}} & \frac{\lambda_4}{2\sqrt{2}} & \frac{\lambda_4}{2\sqrt{2}} & 0 & 0 & 0 & 0 & 0 & 0 & 0 & 0 \\ 0 & \lambda_1 + \frac{\lambda_4}{2} & -\frac{i\lambda_4}{2\sqrt{2}} & \frac{i\lambda_4}{2\sqrt{2}} & \frac{\lambda_4}{2\sqrt{2}} & \frac{i\lambda_4}{2\sqrt{2}} & 0 & 0 & 0 & 0 & 0 & 0 & 0 & 0 \\ \frac{i\lambda_4}{2\sqrt{2}} & -\frac{i\lambda_4}{2\sqrt{2}} & (\lambda_1 + \lambda_4) & 0 & 0 & 0 & 0 & 0 & 0 & 0 & 0 & 0 & 0 & 0 \\ -\frac{i\lambda_4}{2\sqrt{2}} & \frac{i\lambda_4}{2\sqrt{2}} & 0 & \lambda_1 + \lambda_4 & 0 & 0 & 0 & 0 & 0 & 0 & 0 & 0 & 0 & 0 \\ \frac{\lambda_4}{2\sqrt{2}} & \frac{\lambda_4}{2\sqrt{2}} & 0 & 0 & \lambda_1 + \lambda_4 & 0 & 0 & 0 & 0 & 0 & 0 & 0 & 0 & 0 \\ \frac{\lambda_4}{2\sqrt{2}} & \frac{\lambda_4}{2\sqrt{2}} & 0 & 0 & 0 & \lambda_1 + \lambda_4 & 0 & 0 & 0 & 0 & 0 & 0 & 0 & 0 \\ 0 & 0 & 0 & 0 & 0 & 0 & \lambda_{SH} & 0 & 0 & 0 & 0 & 0 & 0 & 0 \\ 0 & 0 & 0 & 0 & 0 & 0 & 0 & \lambda_{S\Delta} & 0 & 0 & 0 & 0 & 0 & 0 \\ 0 & 0 & 0 & 0 & 0 & 0 & 0 & 0 & \lambda_{SH} & 0 & 0 & 0 & 0 & 0 \\ 0 & 0 & 0 & 0 & 0 & 0 & 0 & 0 & 0 & \lambda_{S\Delta} & 0 & 0 & 0 & 0 \\ 0 & 0 & 0 & 0 & 0 & 0 & 0 & 0 & 0 & 0 & \lambda_{SH} & 0 & 0 & 0 \\ 0 & 0 & 0 & 0 & 0 & 0 & 0 & 0 & 0 & 0 & 0 & \lambda_{S\Delta} & 0 & 0 \\ 0 & 0 & 0 & 0 & 0 & 0 & 0 & 0 & 0 & 0 & 0 & 0 & \lambda_{SH} & 0 \\ 0 & 0 & 0 & 0 & 0 & 0 & 0 & 0 & 0 & 0 & 0 & 0 & 0 & \lambda_{S\Delta} \end{pmatrix}. \quad (\text{B1})$$

The second submatrix \mathcal{M}_2 of the scattering whose initial and final states have charge zero is $E_2 = (G^+ G^-, \delta^+ \delta^-, \frac{G^0 G^0}{\sqrt{2}}, \frac{\eta^0 \eta^0}{\sqrt{2}}, \frac{hh}{2}, \frac{\delta^0 \delta^0}{\sqrt{2}}, \delta^{++} \delta^{--}, SS^*)$. All these states have discrete Z_3 charge $X = 0$. One can find

$$\mathcal{M}_2 = \begin{pmatrix} 4\lambda & \lambda_1 + \frac{\lambda_4}{2} & \frac{4\lambda}{2\sqrt{2}} & \frac{\lambda_1}{\sqrt{2}} & \frac{4\lambda}{2\sqrt{2}} & \frac{\lambda_1}{\sqrt{2}} & \lambda_1 + \lambda_4 & \lambda_{SH} \\ \lambda_1 + \frac{\lambda_4}{2} & 4\lambda_2 + 2\lambda_3 & \frac{2\lambda_1 + \lambda_4}{2\sqrt{2}} & \sqrt{2}(\lambda_2 + \lambda_3) & \frac{2\lambda_1 + \lambda_4}{2\sqrt{2}} & \sqrt{2}(\lambda_2 + \lambda_3) & 2(\lambda_2 + \lambda_3) & \lambda_{S\Delta} \\ \frac{4\lambda}{2\sqrt{2}} & \frac{2\lambda_1 + \lambda_4}{2\sqrt{2}} & 3\lambda & \frac{\lambda_1 + \lambda_4}{2} & \lambda & \frac{\lambda_1 + \lambda_4}{2} & \frac{\lambda_1}{\sqrt{2}} & \frac{\lambda_{SH}}{\sqrt{2}} \\ \frac{\lambda_1}{\sqrt{2}} & \sqrt{2}(\lambda_2 + \lambda_3) & \frac{\lambda_1 + \lambda_4}{2} & 3(\lambda_2 + \lambda_3) & \frac{\lambda_1 + \lambda_4}{2} & (\lambda_2 + \lambda_3) & \sqrt{2}\lambda_2 & \frac{\lambda_{S\Delta}}{\sqrt{2}} \\ \frac{4\lambda}{2\sqrt{2}} & \frac{2\lambda_1 + \lambda_4}{2\sqrt{2}} & \lambda & \frac{\lambda_1 + \lambda_4}{2} & 3\lambda & \frac{\lambda_1 + \lambda_4}{2} & \frac{\lambda_1}{\sqrt{2}} & \frac{\lambda_{SH}}{\sqrt{2}} \\ \frac{\lambda_1}{\sqrt{2}} & \sqrt{2}(\lambda_2 + \lambda_3) & \frac{\lambda_1 + \lambda_4}{2} & (\lambda_2 + \lambda_3) & \frac{\lambda_1 + \lambda_4}{2} & 3(\lambda_2 + \lambda_3) & \sqrt{2}\lambda_2 & \frac{\lambda_{S\Delta}}{\sqrt{2}} \\ (\lambda_1 + \lambda_4) & 2(\lambda_2 + \lambda_3) & \frac{\lambda_1}{\sqrt{2}} & \sqrt{2}\lambda_2 & \frac{\lambda_1}{\sqrt{2}} & \sqrt{2}\lambda_2 & 4(\lambda_2 + \lambda_3) & \lambda_{S\Delta} \\ \lambda_{SH} & \lambda_{S\Delta} & \frac{\lambda_{SH}}{\sqrt{2}} & \frac{\lambda_{S\Delta}}{\sqrt{2}} & \frac{\lambda_{SH}}{\sqrt{2}} & \frac{\lambda_{S\Delta}}{\sqrt{2}} & \lambda_{S\Delta} & 4\lambda_S \end{pmatrix}. \quad (\text{B2})$$

The third submatrix \mathcal{M}_3 of the scattering whose initial and final states have charge zero is $E_3 = (hG^0, \delta^0\eta^0, \frac{SS}{\sqrt{2}}, \frac{S^*S^*}{\sqrt{2}})$. The first two states have discrete Z_3 charge $X = 0$, and the states $\frac{S^*S^*}{\sqrt{2}}$ and $\frac{SS}{\sqrt{2}}$ have $X = 2$ and $X = 1$, respectively. One can find

$$\mathcal{M}_3 = \begin{pmatrix} 2\lambda & 0 & 0 & 0 \\ 0 & 2(\lambda_2 + \lambda_3) & 0 & 0 \\ 0 & 0 & \lambda_S & 0 \\ 0 & 0 & 0 & \lambda_S \end{pmatrix}. \quad (\text{B3})$$

The fourth submatrix \mathcal{M}_4 of the scattering whose initial and final states are charge one is $E_4 = (hG^+, \delta^0G^+, G^0G^+, \eta^0G^+, h\delta^+, \delta^0\delta^+, G^0\delta^+, \eta^0\delta^+, \delta^{++}\delta^-, \delta^{++}G^-, SG^+, S\delta^+, S^*G^+, S^*\delta^+)$. The first ten states have discrete Z_3 charge $X = 0$, and the states $SG^+, S\delta^+$ and $S^*G^+, S^*\delta^+$ have $X = 1$ and $X = 2$, respectively. One can find

$$\mathcal{M}_4 = \begin{pmatrix} 2\lambda & 0 & 0 & 0 & 0 & \frac{\lambda_4}{2\sqrt{2}} & 0 & -i\frac{\lambda_4}{2\sqrt{2}} & -\frac{\lambda_4}{2} & 0 & 0 & 0 & 0 & 0 \\ 0 & \lambda_1 & 0 & 0 & \frac{\lambda_4}{2\sqrt{2}} & 0 & i\frac{\lambda_4}{2\sqrt{2}} & 0 & 0 & 0 & 0 & 0 & 0 & 0 \\ 0 & 0 & 2\lambda & 0 & 0 & i\frac{\lambda_4}{2\sqrt{2}} & 0 & \frac{\lambda_4}{2\sqrt{2}} & -i\frac{\lambda_4}{2} & 0 & 0 & 0 & 0 & 0 \\ 0 & 0 & 0 & \lambda_1 & -i\frac{\lambda_4}{2\sqrt{2}} & 0 & \frac{\lambda_4}{2\sqrt{2}} & 0 & 0 & 0 & 0 & 0 & 0 & 0 \\ 0 & \frac{\lambda_4}{2\sqrt{2}} & 0 & -\frac{\lambda_4}{2\sqrt{2}} & \frac{2\lambda_1 + \lambda_4}{2} & 0 & 0 & 0 & 0 & -\frac{\lambda_4}{2} & 0 & 0 & 0 & 0 \\ \frac{\lambda_4}{2\sqrt{2}} & 0 & i\frac{\lambda_4}{2\sqrt{2}} & 0 & 0 & 2(\lambda_2 + \lambda_3) & 0 & 0 & -\sqrt{2}\lambda_3 & 0 & 0 & 0 & 0 & 0 \\ 0 & i\frac{\lambda_4}{2\sqrt{2}} & 0 & \frac{\lambda_4}{2\sqrt{2}} & 0 & 0 & \frac{2\lambda_1 + \lambda_4}{2} & 0 & 0 & -i\frac{\lambda_4}{2} & 0 & 0 & 0 & 0 \\ -i\frac{\lambda_4}{2\sqrt{2}} & 0 & \frac{\lambda_4}{2\sqrt{2}} & 0 & 0 & 0 & 0 & 2(\lambda_2 + \lambda_3) & -i\sqrt{2}\lambda_3 & 0 & 0 & 0 & 0 & 0 \\ -\frac{\lambda_4}{2} & 0 & -i\frac{\lambda_4}{2} & 0 & 0 & -\sqrt{2}\lambda_3 & 0 & -i\sqrt{2}\lambda_3 & 2(\lambda_2 + \lambda_3) & 0 & 0 & 0 & 0 & 0 \\ 0 & 0 & 0 & 0 & -\frac{\lambda_4}{2} & 0 & -i\frac{\lambda_4}{2} & 0 & 0 & \lambda_1 + \lambda_4 & 0 & 0 & 0 & 0 \\ 0 & 0 & 0 & 0 & 0 & 0 & 0 & 0 & 0 & 0 & \lambda_{SH} & 0 & 0 & 0 \\ 0 & 0 & 0 & 0 & 0 & 0 & 0 & 0 & 0 & 0 & 0 & \lambda_{S\Delta} & 0 & 0 \\ 0 & 0 & 0 & 0 & 0 & 0 & 0 & 0 & 0 & 0 & 0 & 0 & \lambda_{SH} & 0 \\ 0 & 0 & 0 & 0 & 0 & 0 & 0 & 0 & 0 & 0 & 0 & 0 & 0 & \lambda_{S\Delta} \end{pmatrix}. \quad (\text{B4})$$

The fifth submatrix \mathcal{M}_5 of the scattering whose initial and final states have charge two is $E_5 = (\frac{G^+G^+}{\sqrt{2}}, \frac{\delta^+\delta^+}{\sqrt{2}}, \delta^+G^+, \delta^{++}\delta^0, \delta^{++}\eta^0, \delta^{++}G^0, \delta^{++}h, \delta^{++}S, \delta^{++}S^*)$. The first seven states have discrete Z_3 charge $X = 0$, and the states $\delta^{++}S$ and $\delta^{++}S^*$ have $X = 1$ and $X = 2$, respectively. One can find

$$\mathcal{M}_5 = \begin{pmatrix} 2\lambda & 0 & 0 & 0 & 0 & 0 & 0 & 0 & 0 \\ 0 & 2\lambda_2 + \lambda_3 & 0 & -\lambda_3 & -i\lambda_3 & 0 & 0 & 0 & 0 \\ 0 & 0 & \frac{2\lambda_1 + \lambda_4}{2} & 0 & 0 & -i\frac{\lambda_4}{2} & -\frac{\lambda_4}{2} & 0 & 0 \\ 0 & -\lambda_3 & 0 & 2\lambda_2 & 0 & 0 & 0 & 0 & 0 \\ 0 & -i\lambda_3 & 0 & 0 & 2\lambda_2 & 0 & 0 & 0 & 0 \\ 0 & 0 & -i\frac{\lambda_4}{2} & 0 & 0 & \lambda_1 & 0 & 0 & 0 \\ 0 & 0 & -\frac{\lambda_4}{2} & 0 & 0 & 0 & \lambda_1 & 0 & 0 \\ 0 & 0 & 0 & 0 & 0 & 0 & 0 & \lambda_{S\Delta} & 0 \\ 0 & 0 & 0 & 0 & 0 & 0 & 0 & 0 & \lambda_{SH} \end{pmatrix}. \quad (\text{B5})$$

The sixth submatrix \mathcal{M}_6 of the scattering whose initial and final states have charge three is $E_6 = (\delta^{++}G^+, \delta^{++}\delta^+)$. All states have discrete Z_3 charge $X = 0$. One can find

$$\mathcal{M}_6 = \begin{pmatrix} \lambda_1 + \lambda_4 & 0 \\ 0 & 2(\lambda_2 + \lambda_3) \end{pmatrix}. \quad (\text{B6})$$

The last submatrix \mathcal{M}_7 of the scattering whose initial and final states have charge four is $E_7 = \frac{\delta^{++}\delta^{++}}{\sqrt{2}}$, and its discrete Z_3 charge $X = 0$. The \mathcal{M}_7 is $2(\lambda_2 + \lambda_3)$.

The eigenvalues e_i^j of the submatrix \mathcal{M}_i can be written as

$$\begin{aligned} e_1^1 &= \lambda_1 + \lambda_4, & e_1^2 &= \lambda_1, & e_1^3 &= \lambda_1 + \frac{3}{2}\lambda_4, & e_1^4 &= \lambda_{SH}, & e_1^5 &= \lambda_{S\Delta}, & e_2^1 &= 2\lambda, & e_2^2 &= 2\lambda_2, & e_2^3 &= 2(\lambda_2 + \lambda_3), \\ e_2^4 &= \lambda + \lambda_2 + 2\lambda_3 + \sqrt{\lambda^2 - 2\lambda\lambda_2 + \lambda_2^2 - 4\lambda\lambda_3 + 4\lambda_2\lambda_3 + 4\lambda_3^2 + \lambda_4^2}, \\ e_2^5 &= \lambda + \lambda_2 + 2\lambda_3 - \sqrt{\lambda^2 - 2\lambda\lambda_2 + \lambda_2^2 - 4\lambda\lambda_3 + 4\lambda_2\lambda_3 + 4\lambda_3^2 + \lambda_4^2}, \\ e_2^6 &= \frac{1}{4}\text{Root}[A], & e_3^1 &= 2\lambda, & e_3^2 &= 2(\lambda_2 + \lambda_3), & e_3^3 &= \lambda_S, & e_4^1 &= \lambda_1 + \lambda_4, & e_4^2 &= \lambda_1, \\ e_4^3 &= \lambda_1 + \frac{3\lambda_4}{2}, & e_4^4 &= 2\lambda, & e_4^5 &= 2\lambda_2, & e_4^6 &= 2(\lambda_2 + \lambda_3), & e_4^7 &= \lambda_1 - \frac{\lambda_4}{2}, \\ e_4^8 &= \frac{1}{4} \left[4\lambda + 4\lambda_2 + 8\lambda_3 + \sqrt{(4\lambda - 4\lambda_2 - 8\lambda_3)^2 + 16\lambda_4^2} \right], \\ e_4^9 &= \frac{1}{4} \left[4\lambda + 4\lambda_2 + 8\lambda_3 - \sqrt{(4\lambda - 4\lambda_2 - 8\lambda_3)^2 + 16\lambda_4^2} \right], \\ e_4^{10} &= \lambda_{SH}, & e_4^{11} &= \lambda_{S\Delta}, & e_5^1 &= \lambda_1 + \lambda_4, & e_5^2 &= \lambda_1, & e_5^3 &= 2\lambda, & e_5^4 &= 2\lambda_2, & e_5^5 &= 2(\lambda_2 + \lambda_3), \\ e_5^6 &= \lambda_1 - \frac{\lambda_4}{2}, & e_5^7 &= 2\lambda_2 - \lambda_3, & e_5^8 &= \lambda_{S\Delta}, & e_5^9 &= \lambda_1 + \lambda_4, & e_5^{10} &= 2(\lambda_2 + \lambda_3), & e_5^{11} &= 2(\lambda_2 + \lambda_3), \end{aligned} \quad (\text{B7})$$

where we have ignored duplicate eigenvalues for \mathcal{M}_i . The symbol $\text{Root}[A]$ stands for the roots of the cubic equation, and we will apply Sanmuelson's inequality [92] to place the restrictions on the region of roots,

$$\begin{aligned} &x^3 + x^2(-24\lambda - 32\lambda_2 - 24\lambda_3 - 16\lambda_S) + x(-96\lambda_1^2 + 768\lambda\lambda_2 + 576\lambda\lambda_3 - 100\lambda_1\lambda_4 - 26\lambda_4^2) \\ &+ 1536\lambda_1^2\lambda_S - 12288\lambda_2\lambda_3\lambda_S - 9216\lambda\lambda_3\lambda_S + 1600\lambda_1\lambda_4\lambda_S + 416\lambda_4^2\lambda_S + 1152\lambda\lambda_{S\Delta}^2 \\ &- 768\lambda_1\lambda_{S\Delta}\lambda_{SH} - 400\lambda_4\lambda_{S\Delta}\lambda_{SH} + 1024\lambda_2\lambda_{SH}^2 + 768\lambda_3\lambda_{SH}^2 = 0. \end{aligned} \quad (\text{B8})$$

- [1] F. Zwicky, *Helv. Phys. Acta* **6**, 110 (1933).
- [2] S. W. Allen, A. E. Evrard, and A. B. Mantz, *Annu. Rev. Astron. Astrophys.* **49**, 409 (2011).
- [3] V. C. Rubin, N. Thonnard, and W. K. Ford, Jr., *Astrophys. J.* **238**, 471 (1980).
- [4] C. S. Frenk and S. D. M. White, *Ann. Phys. (Amsterdam)* **524**, 507 (2012).
- [5] A. Refregier, *Annu. Rev. Astron. Astrophys.* **41**, 645 (2003).
- [6] G. Hinshaw *et al.* (WMAP Collaboration), *Astrophys. J. Suppl. Ser.* **208**, 19 (2013).
- [7] K. A. Olive, *Chin. Phys. C* **38**, 090001 (2014).
- [8] S.-M. Choi and H. M. Lee, *J. High Energy Phys.* **09** (2015) 063.
- [9] Y. Hochberg, E. Kuflik, T. Volansky, and J. G. Wacker, *Phys. Rev. Lett.* **113**, 171301 (2014).
- [10] Y. Hochberg, E. Kuflik, H. Murayama, T. Volansky, and J. G. Wacker, *Phys. Rev. Lett.* **115**, 021301 (2015).
- [11] H. M. Lee and M.-S. Seo, *Phys. Lett. B* **748**, 316 (2015).
- [12] S.-M. Choi, Y.-J. Kang, and H. M. Lee, *J. High Energy Phys.* **12** (2016) 099.
- [13] R. T. D'Agnolo and J. T. Ruderman, *Phys. Rev. Lett.* **115**, 061301 (2015).
- [14] P. Minkowski, *Phys. Lett.* **67B**, 421 (1977).
- [15] T. Yanagida, KEK Report No. KEK-79-18, 1979, p. 95.
- [16] R. N. Mohapatra and G. Senjanovic, *Phys. Rev. Lett.* **44**, 912 (1980).
- [17] M. Magg and C. Wetterich, *Phys. Lett.* **94B**, 61 (1980).
- [18] G. Lazarides, Q. Shafi, and C. Wetterich, *Nucl. Phys.* **B181**, 287 (1981).
- [19] D. Ashery, I. Navon, G. Azuelos, H. K. Walter, H. J. Pfeiffer, and F. W. Schlegel, *Phys. Rev. C* **23**, 2173 (1981).
- [20] E. Ma and U. Sarkar, *Phys. Rev. Lett.* **80**, 5716 (1998).
- [21] W. Konetschny and W. Kummer, *Phys. Lett.* **70B**, 433 (1977).
- [22] J. Schechter and J. W. F. Valle, *Phys. Rev. D* **22**, 2227 (1980).
- [23] T. P. Cheng and L.-F. Li, *Phys. Rev. D* **22**, 2860 (1980).
- [24] S. M. Bilenky, J. Hosek, and S. T. Petcov, *Phys. Lett.* **94B**, 495 (1980).
- [25] E. Ma, *Phys. Rev. Lett.* **81**, 1171 (1998).
- [26] B. Bajc and G. Senjanovi, *J. High Energy Phys.* **08** (2007) 014.
- [27] P. F. Pérez, *Phys. Lett. B* **654**, 189 (2007).
- [28] P. Fileviez Perez, *Phys. Rev. D* **76**, 071701 (2007).
- [29] N. G. Deshpande and E. Ma, *Phys. Rev. D* **18**, 2574 (1978).
- [30] E. Ma, *Phys. Rev. D* **73**, 077301 (2006).
- [31] R. Barbieri, L. J. Hall, and V. S. Rychkov, *Phys. Rev. D* **74**, 015007 (2006).
- [32] L. Lopez Honorez, E. Nezri, J. F. Oliver, and M. H. G. Tytgat, *J. Cosmol. Astropart. Phys.* **02** (2007) 028.
- [33] G. Bélanger, K. Kannike, A. Pukhov, and M. Raidal, *J. Cosmol. Astropart. Phys.* **06** (2014) 021.
- [34] G. Belanger, K. Kannike, A. Pukhov, and M. Raidal, *J. Cosmol. Astropart. Phys.* **04** (2012) 010.
- [35] B. D. Sáez and K. Ghorbani, *J. Cosmol. Astropart. Phys.* **02** (2023) 002.
- [36] S. P. Martin, *Phys. Rev. D* **46**, R2769 (1992).
- [37] L. M. Krauss and F. Wilczek, *Phys. Rev. Lett.* **62**, 1221 (1989).
- [38] G. Belanger, K. Kannike, A. Pukhov, and M. Raidal, *J. Cosmol. Astropart. Phys.* **01** (2013) 022.
- [39] P. Ko and Y. Tang, *J. Cosmol. Astropart. Phys.* **05** (2014) 047.
- [40] N. Bernal, C. Garcia-Cely, and R. Rosenfeld, *J. Cosmol. Astropart. Phys.* **04** (2015) 012.
- [41] A. Hektor, A. Hryczuk, and K. Kannike, *J. High Energy Phys.* **03** (2019) 204.
- [42] M. Aguilar *et al.* (AMS Collaboration), *Phys. Rev. Lett.* **113**, 121102 (2014).
- [43] S. Abdollahi *et al.* (Fermi-LAT Collaboration), *Phys. Rev. D* **95**, 082007 (2017).
- [44] DAMPE Collaboration, *Nature (London)* **552**, 63 (2017).
- [45] P. S. B. Dev, D. K. Ghosh, N. Okada, and I. Saha, *Phys. Rev. D* **89**, 095001 (2014).
- [46] T. Li, N. Okada, and Q. Shafi, *Phys. Lett. B* **779**, 130 (2018).
- [47] T. Li, N. Okada, and Q. Shafi, *Phys. Rev. D* **98**, 055002 (2018).
- [48] M. Aguilar *et al.* (AMS Collaboration), *Phys. Rep.* **366**, 331 (2002); **380**, 97(E) (2003).
- [49] O. Adriani *et al.* (PAMELA Collaboration), *Phys. Rev. Lett.* **105**, 121101 (2010).
- [50] M. Ibe, H. Murayama, and T. T. Yanagida, *Phys. Rev. D* **79**, 095009 (2009).
- [51] J. D. March-Russell and S. M. West, *Phys. Lett. B* **676**, 133 (2009).
- [52] W.-L. Guo and Y.-L. Wu, *Phys. Rev. D* **79**, 055012 (2009).
- [53] A. Arhrib, R. Benbrik, M. Chabab, G. Moulhaka, M. C. Peyranere, L. Rahili, and J. Ramadan, *Phys. Rev. D* **84**, 095005 (2011).
- [54] P. Fileviez Perez, T. Han, G.-y. Huang, T. Li, and K. Wang, *Phys. Rev. D* **78**, 015018 (2008).
- [55] P. Fileviez Perez, T. Han, G.-Y. Huang, T. Li, and K. Wang, *Phys. Rev. D* **78**, 071301 (2008).
- [56] R. N. Lerner and J. McDonald, *Phys. Rev. D* **80**, 123507 (2009).
- [57] A. Schuessler and D. Zeppenfeld, *High Energy Phys. Phenom.* 236 (2007), arXiv:0710.5175.
- [58] K. Kannike, *Eur. Phys. J. C* **72**, 2093 (2012).
- [59] K. P. Hadeler, *Linear Algebra Appl.* **49**, 79 (1983).
- [60] G. Chang and T. W. Sederberg, *Comput. Aided Geom. Des.* **11**, 113 (1994).
- [61] G. Bélanger, F. Boudjema, A. Goudelis, A. Pukhov, and B. Zaldivar, *Comput. Phys. Commun.* **231**, 173 (2018).
- [62] A. Alloul, N. D. Christensen, C. Degrande, C. Duhr, and B. Fuks, *Comput. Phys. Commun.* **185**, 2250 (2014).
- [63] P. A. R. Ade *et al.* (Planck Collaboration), *Astron. Astrophys.* **594**, A13 (2016).
- [64] Y. Meng *et al.* (PandaX-4T Collaboration), *Phys. Rev. Lett.* **127**, 261802 (2021).
- [65] Q. Yuan *et al.*, arXiv:1711.10989.
- [66] N. Okada and O. Seto, *Mod. Phys. Lett. A* **33**, 1850157 (2018).
- [67] L. Randall and W. L. Xu, *J. High Energy Phys.* **05** (2020) 081.
- [68] S. Yaser Ayazi and A. Mohamadnejad, *J. Phys. G* **47**, 095003 (2020).
- [69] M. Kachelriess and D. V. Semikoz, *Prog. Part. Nucl. Phys.* **109**, 103710 (2019).

- [70] L. Feng, Z. Kang, Q. Yuan, P.-F. Yin, and Y.-Z. Fan, *J. Cosmol. Astropart. Phys.* **04** (2020) 031.
- [71] C. V. Cappiello, K. C. Y. Ng, and J. F. Beacom, *Phys. Rev. D* **99**, 063004 (2019).
- [72] Q. Yuan and L. Feng, *Sci. China Phys. Mech. Astron.* **61**, 101002 (2018).
- [73] C.-H. Chen, C.-W. Chiang, and T. Nomura, *Phys. Rev. D* **97**, 061302 (2018).
- [74] X. Liu and Z. Liu, *Phys. Rev. D* **98**, 035025 (2018).
- [75] H.-B. Jin, B. Yue, X. Zhang, and X. Chen, *Phys. Rev. D* **98**, 123008 (2018).
- [76] T. Bringmann and P. Salati, *Phys. Rev. D* **75**, 083006 (2007).
- [77] E. A. Baltz and J. Edsjo, *Phys. Rev. D* **59**, 023511 (1998).
- [78] E. A. Baltz, J. Edsjo, K. Freese, and P. Gondolo, *Phys. Rev. D* **65**, 063511 (2002).
- [79] I. V. Moskalenko and A. W. Strong, *Astrophys. J.* **493**, 694 (1998).
- [80] M. Aguilar *et al.* (AMS Collaboration), *Phys. Rev. Lett.* **110**, 141102 (2013).
- [81] Y. Asaoka *et al.*, *Phys. Rev. Lett.* **88**, 051101 (2002).
- [82] P. S. Bhupal Dev, D. K. Ghosh, N. Okada, and I. Saha, *J. High Energy Phys.* **03** (2013) 150; **05** (2013) 49(E).
- [83] G. Elor, N. L. Rodd, T. R. Slatyer, and W. Xue, *J. Cosmol. Astropart. Phys.* **06** (2016) 024.
- [84] C. Patrignani, *Phys. Lett.* **40B**, 100001 (2016).
- [85] C.-H. Chen and T. Nomura, *J. High Energy Phys.* **09** (2014) 120.
- [86] I. Esteban, M. C. Gonzalez-Garcia, M. Maltoni, I. Martinez-Soler, and T. Schwetz, *J. High Energy Phys.* **01** (2017) 087.
- [87] A. Belyaev, N. D. Christensen, and A. Pukhov, *Comput. Phys. Commun.* **184**, 1729 (2013).
- [88] A. G. Akeroyd, M. Aoki, and H. Sugiyama, *Phys. Rev. D* **79**, 113010 (2009).
- [89] T. Fukuyama, H. Sugiyama, and K. Tsumura, *J. High Energy Phys.* **03** (2010) 044.
- [90] M. Aaboud *et al.* (ATLAS Collaboration), *Eur. Phys. J. C* **78**, 199 (2018).
- [91] G. Aad *et al.* (ATLAS Collaboration), *J. High Energy Phys.* **03** (2015) 041.
- [92] P. A. Samuelson, *J. Am. Stat. Assoc.* **63**, 1522 (1968).